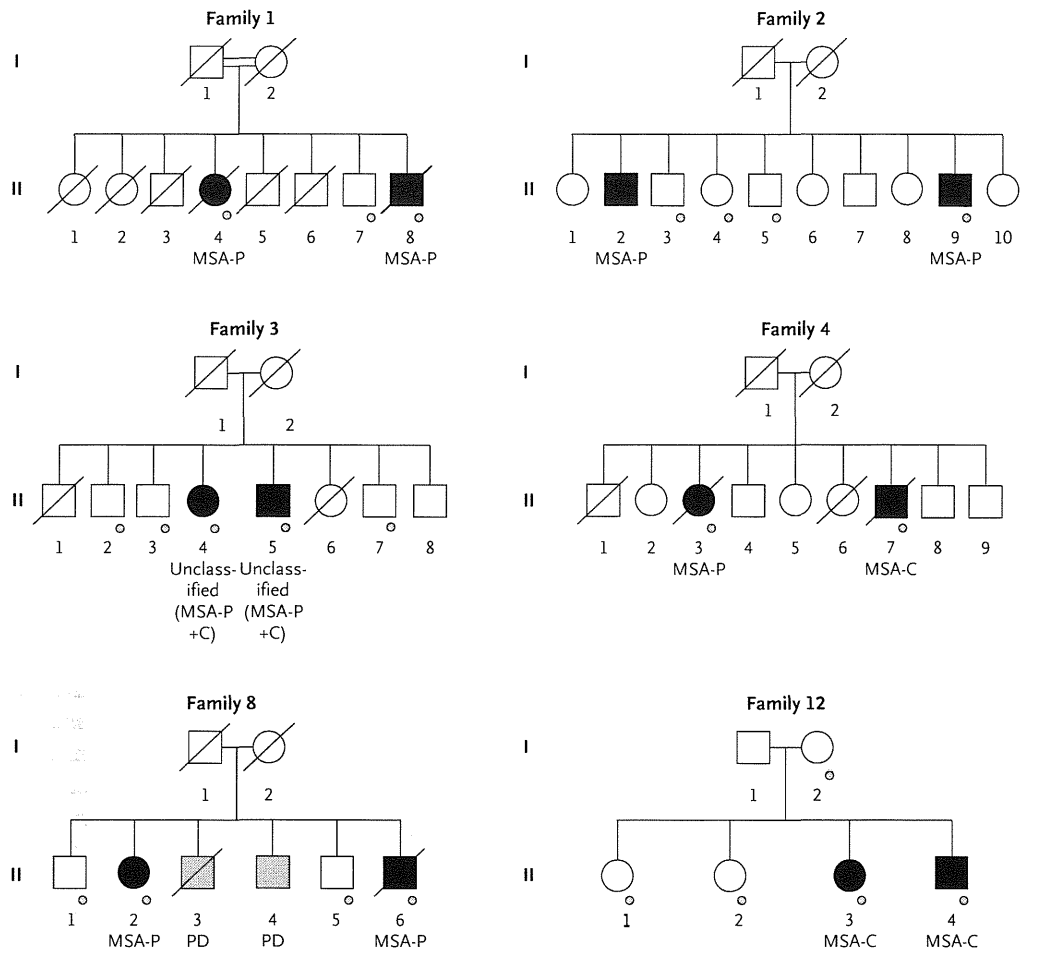

Figure 1. Pedigrees of Six Multiplex Families with Multiple-System Atrophy.

The affected siblings in Family 1 were born to consanguineous parents (first cousins).[13] In this family, the two patients with multiple-system atrophy (Participants II-4 and II-8) also had retinitis pigmentosa, which was not present in the other siblings. The diagnosis of definite multiple-system atrophy in three patients (Participants II-4 and II-8 in Family 1 and II-6 in Family 8) was confirmed at autopsy. In Family 8, two siblings (Participants II-3 and II-4) of the affected family members had Parkinson's disease (PD). In Family 1, in which homozygous M78V-V343A mutations in *COQ2* were identified, the parents (Participants I-1 and I-2), who were obligate carriers of the mutation, showed no overt signs of parkinsonism, cerebellar ataxia, or autonomic dysfunction, according to family report. In Family 12, in whom compound heterozygous R337X/V343A mutations were identified, Participants I-1 and I-2 (obligate carriers of the mutations) and the heterozygous carrier (Participant II-2) showed no overt signs of parkinsonism, cerebellar ataxia, or autonomic dysfunction on examination by a neurologist. Squares represent male family members, circles female family members, black symbols family members with multiple-system atrophy, gray symbols family members with Parkinson's disease, open symbols unaffected family members, slashes deceased family members, and small circles family members for whom genomic DNA samples were available. MSA-C denotes multiple-system atrophy of the cerebellar type, MSA-P multiple-system atrophy with predominant parkinsonism, and unclassified MSA-P+C similarly predominant parkinsonian and cerebellar signs.

ANALYSIS OF *COQ2* AND OTHER GENES ASSOCIATED WITH COENZYME Q_{10}

On the basis of linkage analysis and whole-genome sequencing, we sequenced *COQ2* and the other 11 genes involved in the biosynthetic pathway for coenzyme Q_{10} (*PDSS1*, *PDSS2*, *COQ3*, *COQ4*, *COQ5*, *COQ6*, *COQ7*, *ADCK3*, *COQ9*, *COQ10A*, and *COQ10B*), using the Sanger method (Table S3 in the Supplementary Appendix).

We prepared samples of mutant human *COQ2* complementary DNA (cDNA) by means of site-directed mutagenesis (Table S4 in the Supple-

mentary Appendix). A yeast *coq2*-null mutant, the BY4741Δ*coq2* strain, was transformed with pAUR123 (Takara Bio) containing the nonmutated or mutated human *COQ2* cDNA. We measured the growth rate in a medium with a nonfermentable carbon source by monitoring the optical density of a sample measured at a wavelength of 600 nm (OD_{600}). We used mitochondrial fractions prepared from lymphoblastoid cell lines with the QProteome Mitochondria Isolation Kit (Qiagen) as the enzyme source. COQ2 activity (Enzyme Commission number, 2.5.1.39) was assayed as described previously.[20]

COENZYME Q_{10} LEVEL IN TISSUES

Using high-performance liquid chromatography, we measured levels of coenzyme Q_{10} (ubiquinone-10 and ubiquinol-10) and free (unesterified) cholesterol in lymphoblastoid cell lines established from 152 patients with multiple-system atrophy and 76 controls and in cerebellum samples obtained on autopsy from 3 patients with multiple-system atrophy and 3 controls.[21]

STATISTICAL ANALYSIS

All results are presented as means and standard deviations. We used Student's t-test to evaluate the significance of differences in the mean age at disease onset between carriers and noncarriers of the *COQ2* mutation. We used Fisher's exact test to calculate the significance of the difference in allele frequencies between carriers and noncarriers, with contingency tables and standard methods used to compute odds ratios and corresponding 95% confidence intervals. We used the Kruskal–Wallis test, followed by the Steel test, to perform an analysis of variance. All statistical tests were two-sided, and a P value of less than 0.05 was considered to indicate statistical significance.

RESULTS

LINKAGE ANALYSIS OF FAMILIAL DISEASE

Parametric linkage analysis of the six family pedigrees revealed no single locus showing a linkage compatible with autosomal recessive inheritance. However, in the parametric linkage analysis allowing for heterogeneity, we detected several loci showing positive scores for heterogeneity logarithm of the odds (HLOD), indicating that more than one locus was involved in the different multiplex families (Fig. S1B in the Supplementary Appendix). In particular, two regions on chromosome 4 showed the highest HLOD scores, exceeding 2.0. Results of nonparametric linkage analysis (Fig. S1C in the Supplementary Appendix) were consistent with those of parametric linkage analysis allowing for heterogeneity. Parametric linkage analysis of chromosome 4 in individual pedigrees revealed positive LOD scores in an overlapping region in four families (Family 1, Family 2, Family 4, and Family 12), with Family 1 having the highest LOD score of 1.93 (72.795 to 89.616 Mb) (Fig. S1A and S2A in the Supplementary Appendix). Thus, we selected Family 1 to undergo whole-genome sequencing.

SUSCEPTIBILITY GENE IN FAMILIAL DISEASE

Whole-genome sequencing of a sample obtained from Participant II-4, one of two affected members of Family 1, generated 187.5 Gb of short reads, with an average coverage of 58× and 3,492,429 single-nucleotide variants (SNVs) or insertions or deletions. We winnowed the 3,492,429 variants down to 4 by selecting SNVs that were located in the candidate regions defined on linkage analysis in Family 1 (regions with the highest LOD score spanning approximately 80 Mb in total), that were located in exons or splice sites, that were predicted to cause amino acid changes or changes in pre-messenger RNA splicing, and that were not registered in the database of single-nucleotide polymorphisms, build 130 (dbSNP130), indicating that the variants are extremely rare in the general population (Fig. S2B in the Supplementary Appendix). Each of these 4 SNVs is predicted to result in an amino acid substitution: K707R in SHROOM3 (Universal Protein Resource [UniProt] accession number, Q8TF72), M78V and V343A in COQ2 (UniProt accession number, Q96H96), and R231G in SCEL (UniProt accession number, O95171).

In the 180 Japanese control samples, we did not observe the SNV encoding the M78V variant but did observe SNVs encoding K706R in SHROOM3, V343A in COQ2, and R231G in SCEL, which were present on 3, 5, and 98 of 360 alleles, respectively. We therefore considered the SNP encoding M78V in *COQ2*, which encodes parahydroxybenzoate-polyprenyl transferase, an enzyme involved in the biosynthesis of coenzyme Q_{10}, as a candidate variant in conferring susceptibility to familial multiple-system atrophy.

Cosegregation analysis of samples from Family 1 revealed that the two affected family members, Participants II-4 and II-8, carried the homozygous M78V-V343A variant in *COQ2*, and the unaffected sibling who was tested (Participant II-7) did not carry this variant (Fig. S2C in the Supplementary Appendix). Mutational analysis of *COQ2* in Family 12 revealed heterozygous mutations consisting of nonsense (R337X) and missense (V343A) variants in both affected siblings (Participants II-3 and II-4). Their mother (Participant I-2) was heterozygous for V343A, one unaffected sibling (Participant II-1) lacked this variant, and the other unaffected sibling (Participant II-2) was heterozygous for R337X. R337X was not observed in the 180 Japanese controls.

We did not detect variants of *COQ2* in the other four families (Families 2, 3, 4, and 8). Because *COQ2* encodes an enzyme essential for the biosynthesis of coenzyme Q_{10}, we further sequenced the other 11 genes in the biosynthetic pathway for coenzyme Q_{10} (*PDSS1*, *PDSS2*, *COQ3*, *COQ4*, *COQ5*, *COQ6*, *COQ7*, *ADCK3*, *COQ9*, *COQ10A*, and *COQ10B*) in the remaining four families and in a previously described multiplex family[14] but did not observe variants that cosegregated with disease.

COQ2 VARIANTS AND SPORADIC DISEASE

To investigate the involvement of *COQ2* variants in sporadic multiple-system atrophy, we extended the mutational analysis of *COQ2* to a Japanese series consisting of 363 patients with multiple-system atrophy and 520 controls. A common *COQ2* variant (rs6818847, predicted to result in an amino acid substitution, L16V) with allele frequencies of 0.90 and 0.88 in the Japanese patients with multiple-system atrophy and controls, respectively, was not included in further analysis. Four patients with multiple-system atrophy carried two variants simultaneously (one carried an I97T and a nonmutated [NM] allele at codon 97 and V343A/NM at codon 343, one had R337Q/NM at codon 337 and V343A/NM at codon 343, and two had V343A/V343A), whereas none of the controls had two variants of *COQ2* (Table 1). Sequencing of the subcloned mutated alleles confirmed that R337Q/V343A was present in a compound heterozygous state. We were unable to determine the phase of I97T/V343A, because the distance

Table 1. *COQ2* Variants Found in Patients with Sporadic Multiple-System Atrophy in Japanese, European, and North American Series, as Compared with Controls.*

Genotype	Japanese Series		European Series		North American Series	
	Patients (N=363)	Controls (N=520)	Patients (N=223)	Controls (N=315)	Patients (N=172)	Controls (N=294)
P22L/NM	0	1	0	0	0	0
F29L/NM	0	0	1	0	0	0
P49H†/NM	0	0	0	0	1	0
S57T†/NM	0	0	1	0	0	0
R69H†/NM	0	0	0	0	0	1
I97T‡/V343A§	1	0	0	0	0	0
P107S†/NM	1	0	0	0	0	0
S113F†/NM	1	0	0	0	0	0
T267A‡/NM	0	0	1	0	0	0
S297C‡/NM	0	0	1	0	0	0
N336H/NM	0	1	0	0	0	0
R337Q†/V343A§	1	0	0	0	0	0
V343A§/NM	29	17	0	0	0	0
V343A§/V343A§	2	0	0	0	0	0

* NM denotes nonmutated.
† This variant was deemed to be severely deleterious on yeast complementation assay.
‡ This variant was deemed to be mildly deleterious on yeast complementation assay.
§ This variant had decreased COQ2 activity on enzyme assay.

Table 2. Association between the *COQ2* V343A Variant and Sporadic Multiple-System Atrophy in the Japanese Series.*

V343A Variant†	Patients with Multiple-System Atrophy							Patients with Other Neurologic Diseases		
	Patients (N=363)	Tier 1 Controls (N=520)	Comparison with Tier 1		Tier 2 Controls (N=2383)	Comparison with Tier 2		Alzheimer's Disease (N=2728)	Parkinson's Disease (N=659)	ALS (N=634)
			odds ratio (95% CI)	*P value*		*odds ratio (95% CI)*	*P value*			
Allele frequency — no./total no. (%)	35/726 (4.8)	17/1040 (1.6)	3.05 (1.65–5.85)	1.5×10^{-4}	106/4766 (2.2)	2.23 (1.46–3.32)	6.0×10^{-5}	109/5456 (2.0)	33/1318 (2.5)	31/1268 (2.4)
Heterozygous — no.	31	17			106			105	33	31
Homozygous — no.	2	0			0			2	0	0

* Odds ratios and P values are for the comparisons between patients with multiple-system atrophy and each of the two groups of controls (tier 1 and tier 2). ALS denotes amyotrophic lateral sclerosis, and CI confidence interval.

† In the combined series of Japanese, European, and North American participants, functionally deleterious variants P49H, S57T, R69H, I97T, P107S, S113F, T267A, S297C, and R337Q (as determined on yeast complementation assay) were found in 8 of 1516 alleles (0.53%) in patients with multiple-system atrophy, as compared with 1 of 2258 alleles (0.05%) in controls (odds ratio, 11.97; 95% CI, 1.60 to 531.5; P=0.004).

between I97T and V343A was too large to be amplified by means of polymerase-chain-reaction (PCR) assay in a single fragment, and samples of genomic DNA from the parents were unavailable. We found that 29 patients with multiple-system atrophy and 17 controls were heterozygous for the V343A variant. In addition, we detected four novel heterozygous variants: two in patients with multiple-system atrophy (P107S and S113F) and two in controls (P22L and N336H).

Of the *COQ2* variants, the V343A variant is relatively common in the Japanese population. As shown in Table 2, we found that the V343A allele occurred in 35 of 726 alleles (4.8%) from Japanese patients with multiple-system atrophy and in 17 of 1040 alleles (1.6%) from Japanese controls (odds ratio for patients with multiple-system atrophy, 3.05; 95% confidence interval [CI], 1.65 to 5.85; $P=1.5\times10^{-4}$). Genotyping in the second series of 2383 Japanese controls showed that the V343A variant had an allele frequency of 2.2% (106 of 4766 alleles; odds ratio, 2.23; 95% CI, 1.46 to 3.32; $P=6.0\times10^{-5}$). Genotyping Japanese persons with other neurodegenerative diseases revealed that the V343A allele frequencies were 2.0% (109 of 5456 alleles) among patients with Alzheimer's disease, 2.5% (33 of 1318 alleles) among those with Parkinson's disease, and 2.4% (31 of 1268 alleles) among those with ALS. These allele frequencies did not differ significantly from those in the first or second set of controls, confirming the specificity of the V343A variant in patients with multiple-system atrophy. Two patients with Alzheimer's disease who were found to carry homozygous V343A mutations did not show any signs of parkinsonism, cerebellar ataxia, or autonomic dysfunction.

We then performed genotyping in the European and North American series of patients with multiple-system atrophy. In the European series, we found four singleton *COQ2* variants (encoding amino acid substitutions F29L, S57T, T267A, and S297C) among the patients, whereas none of the controls had any variants in *COQ2*. In the North American series, we found one variant (P49H) in a patient with multiple-system atrophy and one variant (R69H) in a control (Table 1). At the time of recruitment for the study, the carrier of R69H, who was 60 years old, had no signs of parkinsonism, cerebellar ataxia, or autonomic dysfunction, but this participant was unavailable for follow-up assessment. Intriguingly, the V343A

variant, a relatively common variant in the Japanese population, was not observed in patients with multiple-system atrophy or controls in either the European or the North American series.

FUNCTIONAL ANALYSIS OF MUTANT *COQ2*

To determine the functional effect of each variant on the mitochondrial aerobic energy production in which coenzyme Q_{10} plays an essential

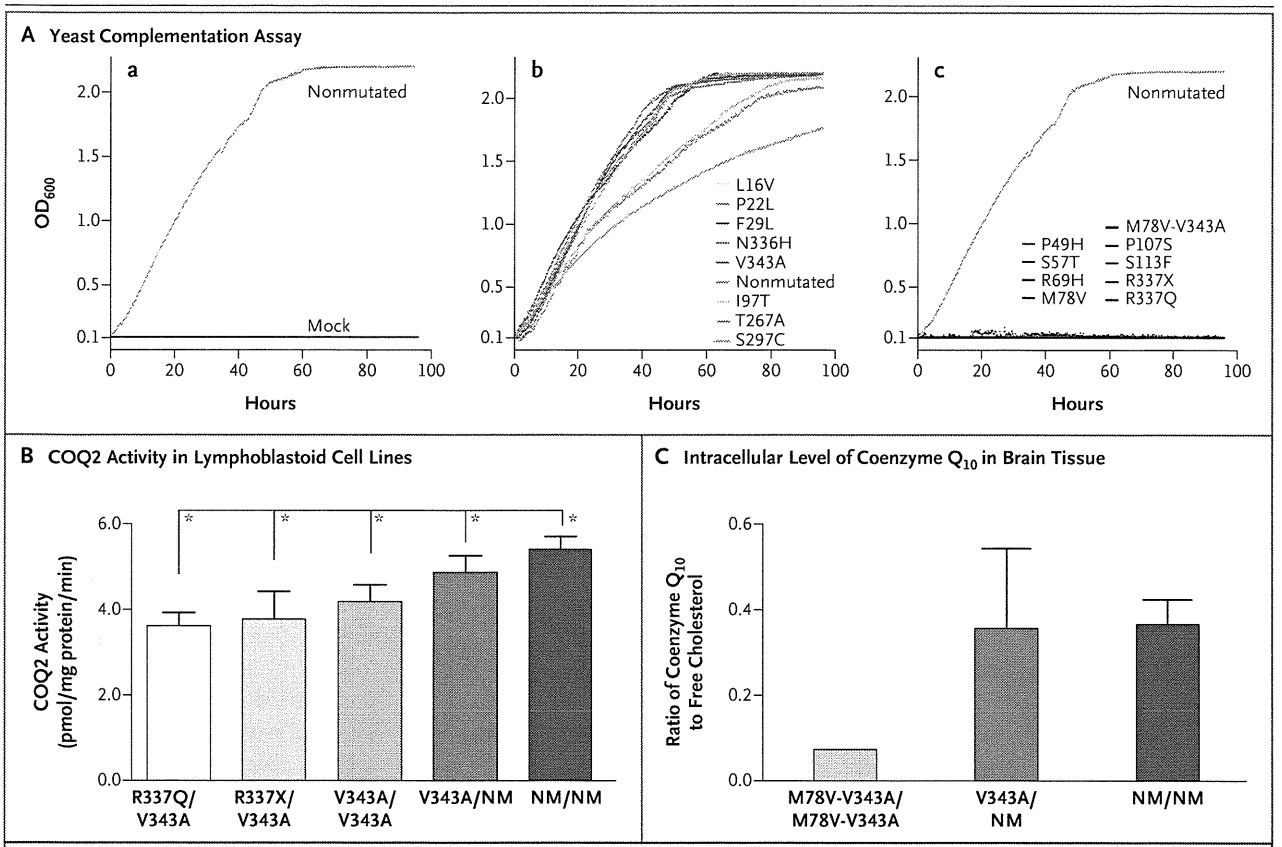

Figure 2. Functional Analysis of *COQ2* Variants.

Panel A shows the results of a yeast complementation assay, including the growth curves of the yeast *coq2*-null mutants transformed with the pAUR123 vector containing the nonmutated (NM) human *COQ2* complementary DNA (cDNA) or mock vector (subpanel a) and those transformed with the AUR123 vector containing different versions of human *COQ2* cDNA (encoding the substitutions L16V, P22L, F29L, N336H, V343A, I97T, T257A, and S297C) (subpanel b). Transformants carrying a *COQ2* allele encoding the I97T, T267A, or S297C substitution show considerably lower growth rates than nonmutated *COQ2*, which still shows a higher growth rate than the *coq2*-null strain (mildly deleterious). Transformants carrying a *COQ2* allele encoding the L16V, P22L, F29L, N336H, or V343A substitution show growth rates similar to that of nonmutated *COQ2*. The *coq2*-null mutants transformed with the pAUR123 vector containing different versions of human *COQ2* cDNA (P49H, S57T, R69H, M78V, M78V-V343A, P107S, S113F, R337X, or R337Q) show severely decreased respiration-dependent growth rates, as does the *coq2*-null strain (severely deleterious) (subpanel c). Each yeast strain was pregrown in yeast extract peptone dextrose (YPD) medium, diluted to an optical density of a sample measured at a wavelength of 600 nm (OD_{600}) of 0.1, and then incubated in yeast extract peptone glycerol (YPG) medium at 23°C with shaking at a rate of 200 rotations per minute for 4 days. OD_{600} was measured every 10 minutes. The experiments were conducted in quadruplicate, and the mean OD_{600} was plotted against the incubation time. Panel B shows COQ2 activity in lymphoblastoid cell lines, as determined by measuring the incorporation of radioactive parahydroxybenzoate (PHB) into decaprenyl-PHB. COQ2 activity was measured in lymphoblastoid cell lines from each patient with multiple-system atrophy carrying *COQ2* variants (encoding R337Q/V343A, R337X/V343A, V343A/V343A, or V343A/NM) and from a control without variants. The mean values from nine independent experiments are shown. T bars indicate standard deviations. Group comparisons were performed with the use of the Kruskal–Wallis test, followed by the Steel test. Asterisks indicate $P<0.05$ for the comparison with a control sample (nonmutated *COQ2* genotype). Panel C shows intracellular levels of coenzyme Q_{10} in frozen cerebellum samples obtained from three patients with multiple-system atrophy (one who was homozygous for M78V-V343A and two who were heterozygous for V343A) and from three controls. Brain-tissue samples weighing approximately 100 mg were homogenized in 10 volumes (volume to weight) of 10 mM TRIS–hydrochloric acid (with a pH of 7.4) containing 0.32 M sucrose, 1 mM ethylenediaminetetraacetic acid (EDTA), and 20% sodium dodecyl sulfate (SDS). Coenzyme Q_{10} was then extracted with hexane and ethanol (in a 5:2 ratio according to volume), and the extract was subjected to high-performance liquid chromatography to measure the level of coenzyme Q_{10}, after adjustment for the free (unesterified) cholesterol level.[21]

role in the electron transfer, we carried out functional complementation analysis by transforming the yeast *coq2*-null strain with nonmutated or mutated human *COQ2* cDNA (Fig. 2A). Transformants of the BY4741 Δ*coq2* yeast strain with the mutated *COQ2*, including transformants separately carrying the P49H, S57T, R69H, M78V, M78V-V343A, P107S, S113F, R337Q, and R337X alleles, showed severely decreased growth rates, similar to those observed in the *coq2*-null strain. In addition, transformants with mutated *COQ2*, including those with the variants encoding the I97T, T267A, and S297C substitutions, showed substantially lower growth rates than those expressing nonmutated *COQ2*, which had a higher growth rate than the *coq2*-null strain (mildly deleterious). The transformants with mutated *COQ2*, including transformants separately carrying the L16V, P22L, F29L, N336H, and V343A alleles, showed growth rates similar to those of the transformants expressing nonmutated *COQ2*. As described above, the yeast strain with M78V-V343A identified in Family 1 showed a severely decreased growth rate, whereas the strain with V343A had a growth rate similar to that of nonmutated *COQ2*, indicating that of the two variants, M78V primarily contributed to the impairment in COQ2 function.

Focusing on the rare variants that were identified in the case–control series (Table 1), we found that nine variants (P49H, S57T, R69H, I97T, P107S, S113F, T267A, S297C, and R337Q) were mildly or severely deleterious. On combining all three series, eight variants (P49H, S57T, I97T, P107S, S113F, T267A, S297C, and R337Q) were identified in 758 patients with multiple-system atrophy, whereas only one variant (R69H) was found in 1129 controls (odds ratio, 11.97; 95% CI, 1.60 to 531.52; P=0.004) (Table 2 footnote). Yeast complementation analysis showed that the F29L variant, identified in a European patient with multiple-system atrophy, did not impair the growth rate. Lymphoblastoid cell lines from this patient were unavailable for further measurement of the activity of mutant COQ2, thus making it difficult to interpret the pathogenicity of this variant.

COQ2 ACTIVITIES IN LYMPHOBLASTOID CELL LINES

We measured COQ2 activities in lymphoblastoid cell lines from patients carrying *COQ2* mutations, when available. We focused on the V343A variant because it is commonly associated with multiple-system atrophy and showed an apparently normal growth rate in the yeast complementation assay. We determined COQ2 activities in lymphoblastoid cell lines with *COQ2* variants R337Q/V343A, R337X/V343A, V343A/V343A, or V343A/NM and in a control without variants. The COQ2 activities in the lymphoblastoid cell lines (V343A/NM) obtained from patients with multiple-system atrophy were significantly lower than those in the control cell lines. The COQ2 activities in the cell lines from patients with multiple-system atrophy carrying two mutated *COQ2* alleles were further decreased (Fig. 2B).

CORRELATIONS BETWEEN GENOTYPE AND PHENOTYPE

The clinical features of patients with sporadic multiple-system atrophy carrying deleterious *COQ2* variants (as determined on yeast complementation assay and COQ2-activity measurement) and those of noncarriers are summarized in Table S5 in the Supplementary Appendix. The mean age at the onset of multiple-system atrophy among carriers was older than that among noncarriers (P=0.002). Among carriers, 34 had subtype C and 5 had subtype P. Among noncarriers, 468 had subtype C and 209 had subtype P. The subtype was unclassified in 42 noncarriers. The ratio of the number of patients with subtype C to the number with subtype P was significantly higher among carriers of *COQ2* variants than among noncarriers (P=0.02).

INTRACELLULAR COENZYME Q_{10} IN LYMPHOBLASTOID CELL LINES

We measured intracellular coenzyme Q_{10} levels in lymphoblastoid cell lines from patients with multiple-system atrophy and controls. The participants were grouped as follows: 3 patients with multiple-system atrophy carrying two variants (R337Q/V343A, R337X/V343A, and V343A/V343A), 16 patients carrying heterozygous V343A, 133 patients without variants, and 76 controls without *COQ2* variants (Table 3). Intracellular levels of coenzyme Q_{10} in lymphoblastoid cell lines from patients with multiple-system atrophy who carried two variant alleles were substantially lower than levels in cell lines from controls without variants. Intracellular coenzyme Q_{10} levels in patients who were heterozygous for V343A and in those without *COQ2* variants were not significantly lower than levels in controls without *COQ2* variants.

Table 3. **Intracellular Levels of Coenzyme Q_{10} in Lymphoblastoid Cell Lines, According to *COQ2* Variant.***

Variable	Patients with Multiple-System Atrophy					Controls
	R337Q/V343A	R337X/V343A	V343A/V343A	V343A/NM	NM/NM	NM/NM
No. of participants with variant	1	1	1	16	133	76
Ratio of coenzyme Q_{10} to free (unesterified) cholesterol†	2.19	2.58	1.86	3.38±0.53	3.41±0.74	3.48±0.75
Coenzyme Q_{10} level as a percentage of mean value in controls — %‡	62.9	74.1	53.4	97.1	98.0	100.0

* Plus–minus values are means ±SD. NM denotes nonmutated.

† The ratio of coenzyme Q_{10} to free (unesterified) cholesterol reflects the intracellular level of coenzyme Q_{10}. Lower values indicate decreased levels of intracellular coenzyme Q_{10}, presumably reflecting decreased biosynthesis of coenzyme Q_{10}. To calculate the ratio, coenzyme Q_{10} was measured in nanomoles per liter and free cholesterol in micromoles per liter.

‡ Lower values indicate decreased levels of intracellular coenzyme Q_{10}, as compared with the mean value in controls, presumably reflecting decreased biosynthesis of coenzyme Q_{10}.

COENZYME Q_{10} IN BRAIN TISSUE

Only a limited number of brain-tissue samples from patients with multiple-system atrophy carrying *COQ2* variants were available. Nevertheless, we measured coenzyme Q_{10} in frozen brain tissues from three patients with *COQ2* variants (one patient who was homozygous for M78V-V343A and two patients with V343A/NM) and from three controls without *COQ2* variants (Fig. 2C). The levels of coenzyme Q_{10} in patients who were homozygous for M78V-V343A were substantially lower than the levels in controls.

DISCUSSION

We identified homozygous or compound heterozygous *COQ2* mutations in two of the six multiplex families with multiple-system atrophy, a finding that suggests a role of these mutations in the pathogenesis of familial disease. We further found that functionally impaired variants in *COQ2* were associated with an increased risk of sporadic disease. In familial cases of multiple-system atrophy, linkage analysis strongly indicated locus heterogeneity in these families, and the identification of the causal variants in the remaining four families will require analyses such as whole-genome sequencing.

We found that a common variant (V343A) and multiple rare variants in *COQ2* were associated with sporadic multiple-system atrophy. The V343A variant was found exclusively in the Japanese participants, with an allele frequency of 1.6 to 2.2%. The allele frequency of V343A in patients with multiple-system atrophy (4.8%) was significantly higher than that in controls (1.6 to 2.2%) with odds ratios of 2.23 to 3.05. The modest risk of multiple-system atrophy that was associated with the common variant V343A suggests that V343A is a susceptibility factor rather than a causal factor for this disease. The odds ratio for the presence of deleterious rare variants was 11.97, which is much larger than that for V343A. Nonetheless, we should consider that these heterozygous variants in *COQ2* are not necessarily causal but rather confer a strong susceptibility to sporadic multiple-system atrophy. Members of Family 1 and Family 12 who carried deleterious variants in the heterozygous state did not have clinical signs of multiple-system atrophy.

The ratio of patients with subtype C multiple-system atrophy to those with subtype P was higher among carriers of deleterious *COQ2* variants than among noncarriers, which suggests that the cerebellum is more vulnerable to compromised COQ2 function than other regions of the central nervous system. Of the *COQ2* variants that we detected, the V343A variant was the most prevalent and was exclusively found in Japanese participants. These findings may in part explain the clinical observations that subtype C is more prevalent than subtype P in the Japanese population[9] but not in the European population[11] or the North American population.[12] However, there were only 35 carriers of deleterious *COQ2* variants among 363 patients with multiple-system atrophy in the Japanese case series. In addition, the clinical presentations of the two patients with familial

disease who had the highest mutational load were different: subtype P in the patients in Family 1 and subtype C in the patients in Family 12. Thus, the genotypes of *COQ2* do not fully explain the clinical phenotypes.

Previous studies have shown evidence of mitochondrial respiratory-chain dysfunction or oxidative injury in patients with multiple-system atrophy.[22-24] The combination of oxidative stress and overexpression of oligodendroglial α-synuclein has been reported to replicate the characteristics of this disease.[25-28] Our findings suggest that impaired COQ2 activity, which would be predicted to impair the mitochondrial respiratory chain and increase vulnerability to oxidative stress, causes susceptibility to multiple-system atrophy. A primary deficiency of coenzyme Q_{10} that is caused by *COQ2* mutations has been described as an infantile-onset multisystem disorder and a nephropathy in several families.[29,30] The clinical presentation of these affected family members, however, differed markedly from the presentations of patients with multiple-system atrophy, perhaps because the decrease in COQ2 activity associated with the mutations in patients with multiple-system atrophy appears to be milder than that observed in patients with a primary deficiency of coenzyme Q_{10}.

Previous approaches to identifying susceptibility genes have used genomewide association studies or candidate-gene approaches.[31-33] Our identification of rare *COQ2* variants was accomplished by starting with multiplex families and then extending the analysis to patients with sporadic multiple-system atrophy, reflecting an alternative approach to the elucidation of genetic variants with strong effect sizes in an apparently nongenetic disorder.[34]

From the therapeutic viewpoint, oral supplementation with coenzyme Q_{10} may be helpful in treating multiple-system atrophy, particularly for patients with susceptibility-conferring *COQ2* variants. The safety and side-effect profile of high-dose supplementation with coenzyme Q_{10} have been well established.[35,36]

Supported in part by grants from the Japan Society for the Promotion of Science (KAKENHI) (22129001 and 22129002, to Dr. Tsuji); the Ministry of Health, Labor, and Welfare of Japan (H23-Jitsuyoka [Nanbyo]-Ippan-004, to Dr. Tsuji); the Japanese Ministry of Education, Culture, Sports, Science, and Technology; the French Agency for Research (ANR-09-MNPS-032-01/R09148DS, to Drs. Dürr and Brice); Programme Hospitalier de Recherche Clinique (AOM03059/R05129DD, to Drs. Dürr and Brice); Deutsche Forschungsgemeinschaft (Wu 184-6, to Dr. Wüllner); and Deutsche Parkinson Vereinigung (to Dr. Wüllner).

Disclosure forms provided by the authors are available with the full text of this article at NEJM.org.

We thank the staff members of the Radioisotope Center at the University of Tokyo; Keiko Hirayama, Zhenghong Wu, and Mio Takeyama for their support in laboratory experiments; Dr. Kazuyuki Tao, Shinya Uchino, and Manabu Seki for their technical help; Dr. Cecilia Marelli for her clinical input; Drs. Yoshinori Kajimoto and Kokoro Ozaki for providing DNA samples and clinical information; and the DNA and Cell Bank of Centre de Recherche de l'Institut du Cerveau et de la Moelle Épinière (CRICM) in Paris for technical assistance.

APPENDIX

The members of the Multiple System Atrophy Research Collaboration are as follows: Jun Mitsui, M.D., Ph.D., Takashi Matsukawa, M.D., and Hiroyuki Ishiura, M.D., Ph.D., Department of Neurology, Graduate School of Medicine, University of Tokyo, Tokyo; Yoko Fukuda, Ph.D., Department of Neurology, Graduate School of Medicine, University of Tokyo, Tokyo, and Max-Planck Institute of Immunobiology and Epigenetics, Freiburg, Germany; Yaeko Ichikawa, M.D., Ph.D., Hidetoshi Date, Ph.D., Budrul Ahsan, Ph.D., Yasuo Nakahara, M.D., Ph.D., Yoshio Momose, M.D., Ph.D., Yuji Takahashi, M.D., Ph.D., Atsushi Iwata, M.D., Ph.D., and Jun Goto, M.D., Ph.D., Department of Neurology, Graduate School of Medicine, University of Tokyo, Tokyo; Yorihiro Yamamoto, Ph.D., School of Bioscience and Biotechnology, Tokyo University of Technology, Tokyo; Makiko Komata, Ph.D., and Katsuhiko Shirahige, Ph.D., Center for Epigenetic Disease, Institute of Molecular and Cellular Biosciences, University of Tokyo, Tokyo; Kenju Hara, M.D., Ph.D., Department of Neurology, Brain Research Institute, Niigata University, Niigata, Japan; Akiyoshi Kakita, M.D., Ph.D., Mitsunori Yamada, M.D., Ph.D., and Hitoshi Takahashi, M.D., Ph.D., Department of Pathology, Brain Research Institute, Niigata University, Niigata, Japan; Osamu Onodera, M.D., Ph.D., and Masatoyo Nishizawa, M.D., Ph.D., Department of Neurology, Brain Research Institute, Niigata University, Niigata, Japan; Hiroshi Takashima, M.D., Ph.D., Department of Neurology and Geriatrics, Kagoshima University Graduate School of Medical and Dental Sciences, Kagoshima, Japan; Ryozo Kuwano, M.D., Ph.D., Department of Molecular Genetics, Center for Bioresources, Brain Research Institute, Niigata University, Niigata, Japan; Hirohisa Watanabe, M.D., Ph.D., Mizuki Ito, M.D., Ph.D., and Gen Sobue, M.D., Ph.D., Department of Neurology, Nagoya University Graduate School of Medicine, Nagoya, Japan; Hiroyuki Soma, M.D., Ph.D., Ichiro Yabe, M.D., Ph.D., and Hidenao Sasaki, M.D., Ph.D., Department of Neurology, Hokkaido University Graduate School of Medicine, Sapporo, Japan; Masashi Aoki, M.D., Ph.D., Department of Neurology, Tohoku University School of Medicine, Sendai, Japan; Kinya Ishikawa, M.D., Ph.D., and Hidehiro Mizusawa, M.D., Ph.D., Department of Neurology and Neurological Science, Graduate School of Medical and Dental Science, Tokyo Medical and Dental University, Tokyo; Kazuaki Kanai, M.D., Ph.D., Takamichi Hattori, M.D., Ph.D., and Satoshi Kuwabara, M.D., Ph.D., Department of Neurology, Chiba University School of Medicine, Chiba, Japan; Kimihito Arai, M.D., Ph.D., Division of Neurology, National Hospital Organization, Chiba East Hospital, Chiba, Japan; Shigeru Koyano, M.D., Ph.D., Department of Clinical Neurology and Stroke Medicine, Graduate School of Medicine, Yokohama City University, Yokohama, Japan; Yoshiyuki Kuroiwa, M.D., Ph.D., Department of Neurology, Teikyo University School of Medicine University Hospital, Mizonokuchi, Kawasaki, Japan; Kazuko Hasegawa, M.D., Ph.D., Division of Neurology, National Hospital Organization, Sagamihara National Hospital, Sagamihara, Japan; Tatsuhiko Yuasa, M.D., Ph.D., Department of Neurology, Kama-

gaya-Chiba Medical Center for Intractable Neurological Disease, Kamagaya General Hospital, Chiba, Japan; Kenichi Yasui, M.D., Ph.D., and Kenji Nakashima, M.D., Ph.D., Division of Neurology, Department of Brain and Neurosciences, Faculty of Medicine, Tottori University, Yonago, Japan; Hijiri Ito, M.D., Ph.D., Department of Neurology, Mifukai Vihara Hananosato Hospital, Hiroshima, Japan; Yuishin Izumi, M.D., Ph.D., and Ryuji Kaji, M.D., Ph.D., Department of Clinical Neuroscience, Institute of Health Biosciences, University of Tokushima Graduate School, Tokushima, Japan; Takeo Kato, M.D., Ph.D., Departments of Neurology, Hematology, Metabolism, Endocrinology, and Diabetology, Faculty of Medicine, Yamagata University, Yamagata, Japan; Susumu Kusunoki, M.D., Ph.D., Department of Neurology, Kinki University School of Medicine, Osaka, Japan; Yasushi Osaki, M.D., Ph.D., Department of Geriatrics, Cardiology and Neurology, Kochi Medical School, Nankoku, Japan; Masahiro Horiuchi, M.D., Ph.D., Division of Neurology, Department of Internal Medicine, St. Marianna University School of Medicine, Kawasaki, Japan; Tomoyoshi Kondo, M.D., Ph.D., Department of Neurology, Wakayama Medical University, Wakayama, Japan; Shigeo Murayama, M.D., Ph.D., Department of Neuropathology and the Brain Bank for Aging Research, Tokyo Metropolitan Geriatric Hospital and Institute of Gerontology, Tokyo; Nobutaka Hattori, M.D., Ph.D., Department of Neurology, Juntendo University School of Medicine, Tokyo; Mitsutoshi Yamamoto, M.D., Ph.D., Department of Neurology, Kagawa Prefectural Central Hospital, Takamatsu, Japan; Miho Murata, M.D., Ph.D., Department of Neurology, National Center Hospital of Neurology and Psychiatry, Tokyo; Wataru Satake, M.D., Ph.D., and Tatsushi Toda, M.D., Ph.D., Division of Neurology/Molecular Brain Science, Kobe University Graduate School of Medicine, Kobe, Japan; Alexandra Dürr, M.D., Ph.D., and Alexis Brice, M.D., INSERM, UMR_S975, CRICM, F-75013, Paris, UPMC University of Paris 06, UMR_S975, F-75013, Paris, CNRS UMR 7225, F-75013, Paris, and Hôpital de la Salpêtrière, Département de Génétique et Cytogénétique, F-75013, Paris; Alessandro Filla, M.D., Department of Neurological Sciences, University Federico II, Naples, Italy; Thomas Klockgether, M.D., and Ullrich Wüllner, M.D., Ph.D., Department of Neurology, University of Bonn and German Center for Neurodegenerative Diseases (DZNE), Bonn, Germany; Garth Nicholson, M.B., B.S., Ph.D., University of Sydney at the Australian and New Zealand Army Corps (ANZAC) Research Institute, Concord Hospital, Sydney; Sid Gilman, M.D., Department of Neurology, University of Michigan, Ann Arbor; Clifford W. Shults, M.D.,* Department of Neurosciences, University of California, San Diego, School of Medicine, La Jolla; Caroline M. Tanner, M.D., Ph.D., Parkinson's Institute, Sunnyvale, CA; Walter A. Kukull, M.D., Department of Epidemiology, University of Washington School of Public Health, Seattle; Virginia M.-Y. Lee, Ph.D., Institute on Aging, Udall Parkinson's Research Center, Center for Neurodegenerative Disease Research and the Department of Pathology and Laboratory Medicine, Perelman School of Medicine at the University of Pennsylvania, Philadelphia; Eliezer Masliah, M.D., Department of Neurosciences, University of California San Diego, San Diego; Phillip A. Low, M.D., and Paola Sandroni, M.D., Ph.D., Department of Neurology, Mayo Clinic, Rochester, MN; John Q. Trojanowski, M.D., Ph.D., Institute on Aging, Udall Parkinson's Research Center, Center for Neurodegenerative Disease Research and the Department of Pathology and Laboratory Medicine, Perelman School of Medicine at the University of Pennsylvania, Philadelphia; Laurie Ozelius, Ph.D., Department of Genetics and Genomic Sciences, Mount Sinai School of Medicine, New York; Tatiana Foroud, Ph.D., Department of Medical and Molecular Genetics, Indiana University School of Medicine, Indiana Alcohol Research Center, Indianapolis; and Shoji Tsuji, M.D., Ph.D., Department of Neurology, Graduate School of Medicine and Medical Genome Center, University of Tokyo, Tokyo.

*Deceased.

REFERENCES

1. Graham JG, Oppenheimer DR. Orthostatic hypotension and nicotine sensitivity in a case of multiple system atrophy. J Neurol Neurosurg Psychiatry 1969;32:28-34.
2. Tu PH, Galvin JE, Baba M, et al. Glial cytoplasmic inclusions in white matter oligodendrocytes of multiple system atrophy brains contain insoluble alpha-synuclein. Ann Neurol 1998;44:415-22.
3. Wakabayashi K, Yoshimoto M, Tsuji S, Takahashi H. Alpha-synuclein immunoreactivity in glial cytoplasmic inclusions in multiple system atrophy. Neurosci Lett 1998;249:180-2.
4. Arima K, Uéda K, Sunohara N, et al. NACP/alpha-synuclein immunoreactivity in fibrillary components of neuronal and oligodendroglial cytoplasmic inclusions in the pontine nuclei in multiple system atrophy. Acta Neuropathol 1998;96:439-44.
5. Spillantini MG, Crowther RA, Jakes R, Cairns NJ, Lantos PL, Goedert M. Filamentous alpha-synuclein inclusions link multiple system atrophy with Parkinson's disease and dementia with Lewy bodies. Neurosci Lett 1998;251:205-8.
6. Papp MI, Kahn JE, Lantos PL. Glial cytoplasmic inclusions in the CNS of patients with multiple system atrophy (striatonigral degeneration, olivopontocerebellar atrophy and Shy-Drager syndrome). J Neurol Sci 1989;94:79-100.
7. Nakazato Y, Yamazaki H, Hirato J, Ishida Y, Yamaguchi H. Oligodendroglial microtubular tangles in olivopontocerebellar atrophy. J Neuropathol Exp Neurol 1990;49:521-30.
8. Gilman S, Wenning GK, Low PA, et al. Second consensus statement on the diagnosis of multiple system atrophy. Neurology 2008;71:670-6.
9. Watanabe H, Saito Y, Terao S, et al. Progression and prognosis in multiple system atrophy: an analysis of 230 Japanese patients. Brain 2002;125:1070-83.
10. Tsuji S, Onodera O, Goto J, Nishizawa M. Sporadic ataxias in Japan — a population-based epidemiological study. Cerebellum 2008;7:189-97.
11. Geser F, Seppi K, Stampfer-Kountchev M. The European Multiple System Atrophy-Study Group (EMSA-SG). J Neural Transm 2005;112:1677-86.
12. May S, Gilman S, Sowell BB, et al. Potential outcome measures and trial design issues for multiple system atrophy. Mov Disord 2007;22:2371-7.
13. Hara K, Momose Y, Tokiguchi S, et al. Multiplex families with multiple system atrophy. Arch Neurol 2007;64:545-51.
14. Wüllner U, Schmitt I, Kammal M, Kretzschmar HA, Neumann M. Definite multiple system atrophy in a German family. J Neurol Neurosurg Psychiatry 2009;80:449-50.
15. Hohler AD, Singh VJ. Probable hereditary multiple system atrophy-autonomic (MSA-A) in a family in the United States. J Clin Neurosci 2012;19:479-80.
16. Fukuda Y, Nakahara Y, Date H, et al. SNP HiTLink: a high-throughput linkage analysis system employing dense SNP data. BMC Bioinformatics 2009;10:121.
17. Gudbjartsson DF, Thorvaldsson T, Kong A, Gunnarsson G, Ingolfsdottir A. Allegro version 2. Nat Genet 2005;37:1015-6.
18. Li H, Durbin R. Fast and accurate short read alignment with Burrows-Wheeler transform. Bioinformatics 2009;25:1754-60.
19. Li H, Handsaker B, Wysoker A, et al. The Sequence Alignment/Map format and SAMtools. Bioinformatics 2009;25:2078-9.
20. Burón MI, Hermán MD, Alcaín FJ, Villalba JM. Stimulation of polyprenyl 4-hydroxybenzoate transferase activity by sodium cholate and 3-[(cholamidopropyl) dimethylammonio]-1-propanesulfonate. Anal Biochem 2006;353:15-21.
21. Yamashita S, Yamamoto Y. Simultaneous detection of ubiquinol and ubiquinone in human plasma as a marker of oxidative stress. Anal Biochem 1997;250:66-73.
22. Blin O, Desnuelle C, Rascol O, et al. Mitochondrial respiratory failure in skel-

etal muscle from patients with Parkinson's disease and multiple system atrophy. J Neurol Sci 1994;125:95-101.
23. Martinelli P, Giuliani S, Lodi R, Iotti S, Zaniol P, Barbiroli B. Failure of brain and skeletal muscle energy metabolism in multiple system atrophy shown by in vivo phosphorous MR spectroscopy. Adv Neurol 1996;69:271-7.
24. Yamashita T, Ando Y, Obayashi K, et al. Oxidative injury is present in Purkinje cells in patients with olivopontocerebellar atrophy. J Neurol Sci 2000;175:107-10.
25. Stefanova N, Reindl M, Neumann M, et al. Oxidative stress in transgenic mice with oligodendroglial alpha-synuclein overexpression replicates the characteristic neuropathology of multiple system atrophy. Am J Pathol 2005;166:869-76.
26. Stefanova N, Georgievska B, Eriksson H, Poewe W, Wenning GK. Myeloperoxidase inhibition ameliorates multiple system atrophy-like degeneration in a transgenic mouse model. Neurotox Res 2012; 21:393-404.
27. Ubhi K, Lee PH, Adame A, et al. Mitochondrial inhibitor 3-nitroproprionic acid enhances oxidative modification of alpha-synuclein in a transgenic mouse model of multiple system atrophy. J Neurosci Res 2009;87:2728-39.
28. Ubhi K, Rockenstein E, Mante M, et al. Alpha-synuclein deficient mice are resistant to toxin-induced multiple system atrophy. Neuroreport 2010;21:457-62.
29. López-Martín JM, Salviati L, Trevisson E, et al. Missense mutation of the COQ2 gene causes defects of bioenergetics and de novo pyrimidine synthesis. Hum Mol Genet 2007;16:1091-7.
30. Diomedi-Camassei F, Di Giandomenico S, Santorelli FM, et al. COQ2 nephropathy: a newly described inherited mitochondriopathy with primary renal involvement. J Am Soc Nephrol 2007;18:2773-80.
31. Sasaki H, Emi M, Iijima H, et al. Copy number loss of (src homology 2 domain containing)-transforming protein 2 (SHC2) gene: discordant loss in monozygotic twins and frequent loss in patients with multiple system atrophy. Mol Brain 2011; 4:24.
32. Al-Chalabi A, Dürr A, Wood NW, et al. Genetic variants of the alpha-synuclein gene SNCA are associated with multiple system atrophy. PLoS One 2009;4(9):e7114.
33. Scholz SW, Houlden H, Schulte C, et al. SNCA variants are associated with increased risk for multiple system atrophy. Ann Neurol 2009;65:610-4. [Erratum, Ann Neurol 2010;67:277.]
34. Tsuji S. Genetics of neurodegenerative diseases: insights from high-throughput resequencing. Hum Mol Genet 2010;19: R65-R70.
35. Ferrante KL, Shefner J, Zhang H, et al. Tolerance of high-dose (3,000 mg/day) coenzyme Q10 in ALS. Neurology 2005; 65:1834-6.
36. Hyson HC, Kieburtz K, Shoulson I, et al. Safety and tolerability of high-dosage coenzyme Q10 in Huntington's disease and healthy subjects. Mov Disord 2010; 25:1924-8.

Neurobiology of Disease

p62/SQSTM1 Differentially Removes the Toxic Mutant Androgen Receptor via Autophagy and Inclusion Formation in a Spinal and Bulbar Muscular Atrophy Mouse Model

Hideki Doi,[1]* Hiroaki Adachi,[1]* Masahisa Katsuno,[1] Makoto Minamiyama,[1] Shinjiro Matsumoto,[1] Naohide Kondo,[1] Yu Miyazaki,[1] Madoka Iida,[1] Genki Tohnai,[1] Qiang Qiang,[1] Fumiaki Tanaka,[1] Toru Yanagawa,[2] Eiji Warabi,[2] Tetsuro Ishii,[2] and Gen Sobue[1]

[1]Department of Neurology, Nagoya University Graduate School of Medicine, Showa-ku, Nagoya 466-8550, Japan, and [2]Faculty of Medicine, University of Tsukuba, Tennoudai, Tsukuba 305-8575, Japan

Polyglutamine (polyQ) diseases are inherited neurodegenerative disorders that are caused by the expansion of trinucleotide CAG repeats in the causative genes. Spinal and bulbar muscular atrophy (SBMA) is an inherited motor neuron disease that is caused by the expansion of a polyQ tract within the androgen receptor (AR). p62 is a ubiquitin- and light-chain 3-binding protein that is known to regulate the degradation of targeted proteins via autophagy and inclusion formation. In this study, we examined the effects of p62 depletion and overexpression on cultured cells and in a transgenic mouse model that overexpressed the mutant AR. Here, we demonstrate that depletion of p62 significantly exacerbated motor phenotypes and the neuropathological outcome, whereas overexpression of p62 protected against mutant AR toxicity in SBMA mice. Depletion of p62 significantly increased the levels of monomeric mutant AR and mutant AR protein complexes in an SBMA mouse model via the impairment of autophagic degradation. In addition, p62 overexpression improved SBMA mouse phenotypes by inducing cytoprotective inclusion formation. Our results demonstrate that p62 provides two different therapeutic targets in SBMA pathogenesis: (1) autophagy-dependent degradation and (2) benevolent inclusion formation of the mutant AR.

Introduction

Polyglutamine (polyQ) diseases are inherited neurodegenerative disorders that are caused by the expansion of trinucleotide CAG repeats in specific genes (Di Prospero and Fischbeck, 2005). Spinal and bulbar muscular atrophy (SBMA) is a motor neuron disease that is caused by the expansion of a polyQ tract within the androgen receptor (AR) (Adachi et al., 2007). SBMA is characterized by motor neuron loss in the spinal cord and brainstem, along with diffuse nuclear accumulation and nuclear inclusions (NIs) of the mutant AR in residual motor neurons and specific visceral organs (Sobue et al., 1989; Li et al., 1998; Adachi et al., 2005). Nuclear and cytoplasmic inclusions are common pathological features in polyQ diseases and colocalize with many components of the ubiquitin–proteasome system (UPS) and autophagy, which raises the possibility that UPS and autophagy might actively degrade components of these inclusions (Buchberger et al., 2010). Furthermore, molecular chaperones also facilitate the refolding or proteolysis of toxic misfolded proteins and could play a role in protecting neuronal cells against the toxic properties of expanded polyQ (Adachi et al., 2009; Labbadia et al., 2011).

Macroautophagy is a process in which cells form double-membrane vesicles called autophagosomes around a portion of the cytoplasm. The protein p62, which is also known as sequestosome-1 (SQSTM1), is an adaptor protein that binds to ubiquitin and the autophagosome membrane light-chain 3 (LC3) in the autophagic degradation pathway (Ichimura et al., 2008). These autophagosomes ultimately fuse with lysosomes, which results in the degradation of their substrates. Specific phosphorylation of p62 at serine 403 in its ubiquitin-associated (UBA) domain increases the affinity between UBA and the polyubiquitin chain, which results in efficiently targeted polyubiquitinated proteins and stabilization of the sequestosome structure (Matsumoto et al., 2011). Although p62 plays a pivotal role in nuclear and cytoplasmic inclusion formation for disease-causative proteins in neurodegenerative disorders (Kuusisto et al., 2001, 2008; Al-Sarraj et al., 2011;

Received June 25, 2012; revised Feb. 27, 2013; accepted March 22, 2013.

Author contributions: H.D., H.A., and G.S. designed research; H.D., H.A., S.M., Y.M., G.T., T.Y., E.W., and T.I. performed research; M.K., M.M., N.K., and Q.Q. contributed unpublished reagents/analytic tools; H.D., H.A., M.I., F.T., and G.S. analyzed data; H.D., H.A., and G.S. wrote the paper.

This work was supported by a Center-of-Excellence grant from the Ministry of Education, Culture, Sports, Science, and Technology of Japan and grants from the Mochida Memorial Foundation for Medical and Pharmaceutical Research. We also thank Dr. Masaaki Komatsu (Protein Metabolism Project, Tokyo Metropolitan Institute of Medical Science, Tokyo, Japan) for kindly providing the vectors containing p62 with mutations and Dr. Diane E. Merry (Departments of Biochemistry and Molecular Biology, Thomas Jefferson University, Philadelphia, PA) for kindly providing the inducible PC12 cells that express wild-type or mutant AR. We thank Miwa Ito and Kazuko Matsuba (Department of Neurology, Nagoya University, Nagoya, Japan) and Noboru Ogiso, Yasutaka Ohya, and Kumiko Yano (Division for Research of Laboratory Animals at the Center for Research of Laboratory Animals and Medical Research Engineering, Nagoya University, Nagoya, Japan) for their technical assistance.

The authors declare no competing financial interests.

*H.D. and H.A. contributed equally to this work.

Correspondence should be addressed to either Dr. Hiroaki Adachi or Dr. Gen Sobue, Department of Neurology, Nagoya University Graduate School of Medicine, 65 Tsurumai-cho, Showa-ku, Nagoya 466-8550, Japan. E-mail: hadachi-ns@umin.org or sobueg@med.nagoya-u.ac.jp.

DOI:10.1523/JNEUROSCI.3021-12.2013

 0270-6474/13/337710-18$15.00/0

King et al., 2011; Troakes et al., 2012), the role of p62 in the pathogenesis of neurodegenerative disorders, including SBMA, has not yet been fully resolved.

In this study, we examined the effect of p62 depletion and overexpression in cultured cells and a transgenic mouse model that overexpresses mutant AR to explore a potential strategy for SBMA therapy. In the SBMA mouse model, depletion of p62 significantly exacerbated physical, behavioral, and neuropathological outcomes, and overexpression of p62 protected against the toxicity of mutant AR. Depletion of p62 significantly increased the accumulation of monomeric mutant ARs and mutant AR protein complexes in SBMA mice via the impairment of autophagic degradation, whereas overexpression of p62 promoted inclusion body formation that was less toxic in the spinal cord and muscle of SBMA mice. Our results demonstrate that p62 exhibits two different therapeutic aspects that are critical components in the autophagy-dependent degradation of the mutant AR and provides harmless inclusion body formation in SBMA pathogenesis.

Materials and Methods

Plasmid constructs and siRNA. pIRESpuro3, which encodes 3xFLAG-tagged mouse p62, and the PB1 p62 mutant (K7A and D69A, M0) plasmids were kindly provided by Dr. Masaaki Komatsu (Laboratory of Frontier Science, Tokyo Metropolitan Institute of Medical Science, Tokyo, Japan). The PB1 p62 mutant (D69A) plasmid with an HA-tag (see Fig. 2*D*), deletion mutant plasmids for p62 (M1–M7; see Fig. 2*E*), and a plasmid with ubiquitin-binding-disrupting mutation (M406V) of p62 with a FLAG tag (see Fig. 2*G*) were generated using a KOD Plus Mutagenesis Kit (Toyobo). The plasmids pCR3.1–AR–24Q and pCR3.1–AR–97Q (Waza et al., 2005) were also used. All of the constructs were verified by DNA sequencing. siRNAs that target p62 were used at a concentration of 10 nM and had the following sequences: 5′-GAAAGTGCATGAGAAGAGAT T-3′ (sense) and 5′-TCTCTTCTCATGCACTTTCTT-3′ (antisense) for the PC12 cells and 5′-CTTGTAGTTGCATCACGTATT-3′ (sense) and 5′-TA CGTGATGCAACTACAAGTT-3′ (antisense) for the Neuro2A cells.

Cell culture and DNA transfection. PC12 Tet-On cells that express human wild-type AR (AR–10Q) or mutant AR (AR–112Q) were kindly provided by Dr. Diane E. Merry (Departments of Biochemistry and Molecular Biology, Thomas Jefferson University, Philadelphia, PA) (Walcott and Merry, 2002). Plasmid DNA and siRNA were transfected into Neuro2A cells, NSC34 cells, or PC12 Tet-On cells using Lipofectamine 2000 (Invitrogen) according to the instructions of the manufacturer. Cells were plated in 6-cm dishes in 5 ml of DMEM/10% FCS with penicillin and streptomycin, and each dish was transfected with 4 μg of plasmid DNA and p62 or control (mock) siRNA. The PC12 cells were cultured in DMEM that contained 10 ng/ml nerve growth factor (NGF) (Alomone Labs), 1 μg/ml doxycycline, and 1 nM dihydrotestosterone (DHT) for the indicated days, as described previously (Walcott and Merry, 2002). Neuro2A cells were cultured in differentiation medium (DMEM/2% FCS; DMEM supplemented with 2% fetal calf serum) that contained retinoic acid (20 μM) and DHT (1 nM) after transfection. The transfection efficiency was 60–70%. The NSC34 cells were cultured in DMEM/10% FCS for 48 h at 37°C under 5% CO_2.

Generation of AR transgenic/p62 knock-out mice and genotyping. p62 knock-out mice in the C57BL/6J (B6) background were kindly provided by Tetsuro Ishii (Graduate School of Comprehensive Human Sciences, University of Tsukuba, Tsukuba, Japan) (Komatsu et al., 2007). Homozygous p62 knock-out females ($p62^{-/-}$ mice) of the B6 strain were mated with male mice of the BDF1/B6 strain that expressed full-length human AR with 24-polyQ tracts (AR–24Q mice, 5–5 line) or 97-polyQ tracts (AR–97Q mice, 7–8 line) to produce a mixed BDF1 and B6 genetic background. First-generation AR–24Q/$p62^{+/-}$ or AR–97Q/$p62^{+/-}$ mice were mated with $p62^{+/-}$ or $p62^{-/-}$ mice to produce all of the combinations and numbers for each analysis. We screened tail DNA by PCR to detect the deletion of the p62 gene using two primer pairs: 5′-CTGCATGTCTTC TCCCATGAC-3′/5′-TAGATACCTAGGTGAGCTCTG-3′ and 5′-CT TACGGGTCCTTTTCCCAAC-3′/5′-TCCTCCTTGCCCAGAAGATAG-3′.

Transgene construction. Full-length human p62 cDNA was generated from total RNA that was extracted from SH-SY5Y cells by reverse transcription (RT)-PCR. Full-length human p62 was constructed by subcloning p62 inserts that were derived from the full-length human p62 cDNA into the pCAGGS vector (Niwa et al., 1991) using PCR. The HA-tagged p62 fragments were then subcloned by mutagenesis methods, and the DNA sequence was confirmed. The final plasmids were digested to remove the transgene (see Fig. 6*A*).

Generation and maintenance of p62 transgenic mice and genotyping. We generated mice that overexpressed p62 by microinjection of the transgene into B6 fertilized eggs; we obtained four founders. Heterozygous p62 transgenic females of the B6 strain were mated with male mice of the BDF1/B6 strain that overexpressed AR–24Q mice (5–5 line) or AR–97Q mice (7–8 line) to produce a mixed BDF1 and B6 genetic background. First-generation AR–24Q/$p62^{(tg/+)}$ or AR–97Q/$p62^{(tg/+)}$ mice were used for each analysis. We screened tail DNA by PCR for the presence of the transgene using the following primers: 5′-AGCTGCCTTGTACCCACA TC-3′ and 5′-AGCGTAATCTGGAACATCGT-3′.

Neurological and behavioral assessments of SBMA model mice. AR–24Q and AR–97Q mice were generated and maintained as described previously (Katsuno et al., 2002). All of the animal experiments were performed in accordance with the National Institutes of Health *Guide for the Care and Use of Laboratory Animals* and under the approval of the Nagoya University Animal Experiment Committee. The AR–97Q male mice exhibited progressive muscular atrophy and weakness in addition to diffuse nuclear staining (DNS) and NIs of the mutant AR. Similar to SBMA patients, these phenotypes were pronounced in male transgenic mice. The mouse rotarod task (Ugo Basile) was performed on a weekly basis, and cage activity was measured weekly using the AB system (Neuroscience), as described previously (Katsuno et al., 2002). Spontaneous motor activity was monitored in 24 h periods; all vertical and horizontal spontaneous movements, including locomotion, rearing, and head movements, were counted and automatically totaled. Grip strength analysis was performed using an MK380M Grip Strength Meter (Muromachi Kikai).

Immunocytochemistry. PC12 Tet-On cells were plated in a collagen-coated four-chamber slide (BD Biosciences) and were cultured in DMEM that contained 10 ng/ml NGF, 1 μg/ml doxycycline, and 1 nM DHT for the indicated days, as described previously (Walcott and Merry, 2002). The cells were also treated with bafilomycin A1 (11707; Sigma) for 16 h and 10 ng/ml leptomycin B (Enzo Diagnostics) for 2 h before harvest and were fixed with 4% paraformaldehyde for 15 min at room temperature. The cells were then treated in formic acid for 5 min at room temperature and were sequentially incubated with anti-p62 antibody (1:1000; PROGEN Biotechnik), anti-LC3 (1:1000; PM046; Medical and Biological Laboratories), and anti-AR (1:1000; Perseus Proteomics) at 4°C overnight. Next, the sections were incubated with Alexa Fluor 647-conjugated goat anti-guinea pig IgG, Alexa Fluor 546-conjugated goat anti-rabbit IgG, and Alexa Fluor 488-conjugated goat anti-mouse IgG (1:1000; Invitrogen) for 1 h at room temperature. The stained sections were imaged using a confocal laser-scanning microscope (LSM 710; Carl Zeiss).

Patients. Tissue was obtained from three patients with clinicopathologically and genetically confirmed SBMA (51–77 years of age; mean age, 65.7 years) and three controls without neurological disease (51–78 years of age; mean age, 64.0 years). These patients were hospitalized and evaluated at Nagoya University Hospital and its affiliated hospitals. The collection of human tissues and their use for this study were approved by the Ethics Committee of Nagoya University Graduate School of Medicine. Informed consent was obtained to use these tissues for research purposes. Paraffin-embedded sections of the spinal cord were processed and examined in the same manner as was used for the transgenic mice.

Immunohistochemistry and histopathology. Mice were deeply anesthetized with pentobarbital sodium and were transcardially perfused with 20 ml of 4% paraformaldehyde fixative in phosphate buffer, pH 7.4. The spinal cord and skeletal muscle tissues were removed, postfixed overnight in 10% phosphate-buffered Formalin, and processed for paraffin

embedding. Sections (6 μm thickness) of the tissue samples were deparaffinized, dehydrated with alcohol, and treated in formic acid for 5 min at room temperature. For the immunohistochemical studies, the paraffin sections were preheated in a microwave oven for 10 min and were blocked with normal animal serum (1:20). The sections were then incubated with anti-expanded polyQ antibody (1:10,000; 1C2; Millipore) and anti-p62 antibody (1:1000; PROGEN Biotechnik) for all of the human tissues and anti-p62 antibody (1:1000; PM045; Medical and Biological Laboratories), anti-glial fibrillary acidic protein (GFAP) antibody (1:1000; Roche Diagnostics), anti-HA antibody (1:500; C29F4; Cell Signaling Technology), and anti-ubiquitin antibody (1:1000; catalog #3936; Cell Signaling Technology) for the mouse tissues. Primary antibodies were probed using a biotinylated anti-species-specific IgG (Vector Laboratories), and the immune complexes were visualized using streptavidin–horseradish peroxidase (Dako) and 3,3-diaminobenzidine (Dojindo) as a substrate. Anti-ubiquitin antibody binding was probed with a labeled polymer of the secondary antibody as part of the Envision system, which contained horseradish peroxidase (Dako). The sections were counterstained with Mayer's hematoxylin. Paraffin-embedded sections (6 μm thickness) of the gastrocnemius muscle were air dried and stained with hematoxylin and eosin. For double-immunofluorescence staining, the sections were blocked with TSA Blocking Reagent (PerkinElmer Life and Analytical Sciences) and were then sequentially incubated with anti-p62 antibody (1:1000; PM045; Medical and Biological Laboratories) and 1C2 antibody (1:10,000; Millipore) at 4°C overnight. The sections were then incubated with Alexa Fluor 488-conjugated goat anti-rabbit IgG (1:1000; Invitrogen) and Alexa Fluor 546-conjugated goat anti-mouse IgG (1:1300; Invitrogen) for 8 h at 4°C. The stained sections were imaged using a confocal laser-scanning microscope (LSM 710; Carl Zeiss).

Quantification of 1C2-positive cells and ubiquitin-positive NIs. To assess 1C2-positive cells and ubiquitin-positive NIs in the ventral horn of the spinal cord, 50 consecutive transverse sections of the thoracic spinal cord were prepared from each individual mouse. Cells positive for 1C2 within the ventral horn of every fifth section were counted as described previously (Adachi et al., 2001). Populations of 1C2-positive cells and ubiquitin-positive NIs were expressed in units of number per square millimeters (see Fig. 5*G*). To examine 1C2-positive cells and ubiquitin-positive NIs in muscle, the number was calculated from counts of 500 fibers in randomly selected areas of individual mice and was expressed as the number per 100 muscle fibers (see Fig. 5*H*). The ratio of the number of cells with NIs or DNS to that of the total number of 1C2-positive cells was calculated (see Fig. 7*B*,*C*). The 1C2 signal intensity of the DNS was analyzed using Image Gauge software version 4.22 (GE Healthcare). The mean signal intensity of DNS was calculated by correcting the signal intensity of all of the 1C2-positive neurons in the spinal cord and all of the 1C2-positive nuclei in the muscle. The relative signal intensity (R.S.I.) of the DNS was computed as the signal intensity of each cell divided by the mean signal intensity of cells without inclusions (see Fig. 7*D*). The quantitative data for six individual mice are expressed as the mean ± SEM.

Protein expression analyses. Forty-eight hours after transfection, the cells were lysed in TNE buffer (10 mM Tris-HCl, pH 7.5, 1% Nonidet P-40, 150 mM NaCl, and 1 mM EDTA), supplemented with 1 mM PMSF and 6 μg/ml aprotinin and centrifuged at 15,000 × *g* for 15 min at 4°C. Thirteen- and 25-week-old mice were exsanguinated under pentobarbital sodium anesthesia, and tissues were snap frozen with powdered CO_2 in acetone. The tissues were homogenized in CelLytic-M Mammalian Cell Lysis/Extraction Reagent (Sigma) with 1 mM PMSF and 6 μg/ml aprotinin and were centrifuged at 2,500 × *g* for 15 min at 4°C. Supernatant protein concentrations were determined using the DC protein assay (Bio-Rad). Aliquots of the supernatant fractions were loaded on 5–20% SDS-PAGE gels, in which each lane contained 7 μg of cell proteins and 80 μg of neural and muscle tissue. To prevent carryover, the pellets were washed with CelLytic-M Mammalian Cell Lysis/Extraction Reagent, followed by sonication and centrifugation. The insoluble pellets were lysed in 300 μl of 8 M urea solution (30 mM Tris, pH 8.5, 2 M Thiourea, 4% CHAPS, and 8 M urea), sonicated, and centrifuged at 25,000 ×*g* for 15 min at 4°C. Aliquots of the supernatant fractions were loaded on 5–20% SDS-PAGE gels. The gels were then transferred to Hybond-P membranes (GE Healthcare) using 25 mM Tris, 192 mM glycine, 0.1% SDS, and 10% methanol as the transfer buffer. Primary antibodies were used at the following concentrations: rabbit anti-AR, 1:1000 (N20; Santa Cruz Biotechnology); rabbit anti-AR, 1:1000 (H280; Santa Cruz Biotechnology); rabbit anti-p62, 1:1000 (PM045; Medical and Biological Laboratories); rabbit anti-LC3 for cells, 1:1000 (PM036; Medical and Biological Laboratories); rabbit anti-LC3 for mouse tissues, 1:2000 (NB600-1384; Novus Biologicals); mouse anti-glyceraldehyde-3-phosphate dehydrogenase (GAPDH), 1:10000 (MAB374; Millipore); rabbit anti-HA, 1:1000 (Y-11; Santa Cruz Biotechnology); and mouse anti-ubiquitin, 1:1000 (catalog #3936; Cell Signaling Technology). Primary antibodies were probed using HRP-conjugated anti-rabbit Ig $F(ab')_2$ and anti-mouse Ig $F(ab')_2$ (1:5000; GE Healthcare) secondary antibodies and were detected using the ECL Plus kit (GE Healthcare). An LAS-3000 imaging system was used to produce digital images and to quantify band intensities, which were then analyzed using Image Gauge software version 4.22 (GE Healthcare). Densitometric values of ARs were normalized to those of endogenous GAPDH. The R.S.I. was computed as the signal intensity of each sample divided by that of the nontreated cells and control siRNA-transfected cells (see Figs. 1, 3) or the signal intensities of AR–24Q/$p62^{+/+}$ or AR–97Q/$p62^{+/+}$ mice (see Fig. 5) and AR–24Q/$p62^{(+/+)}$ or AR–97Q/$p62^{(+/+)}$ mice (see Fig. 9).

Immunoprecipitation assay. We constructed p62 deletion mutant plasmids using a mutagenesis method with the appropriate primers. Each construct was designed against the functional domains and exons of the corresponding mouse p62 gene to assess which domain of p62 was required for the interaction with the AR (see Fig. 2*E*). Neuro2A cells transfected with AR–24Q and/or AR–97Q and the mutant p62 vectors were lysed. The sample, which contained 0.5 mg of total protein in 500 μl of TNE buffer, was rotated with 40 μl of anti-FLAG M2 agarose beads (Sigma) for 8 h at 4°C. The protein was eluted from the beads using 3xFLAG peptide (Sigma) under native conditions. Anti-HA tag monoclonal antibody magnetic beads (M132-9; Medical and Biological Laboratories), rabbit anti-AR (N20; Santa Cruz Biotechnology), and rabbit anti-p62 (PM045; Medical and Biological Laboratories) with 50 μl of protein G Dynabeads (Invitrogen) was also used in an immunoprecipitation assay. The supernatants were then boiled for 5 min in SDS sample buffer supplemented with 2-mercaptoethanol and loaded on to SDS-polyacrylamide gels. The blots were probed as described for Western blots with anti-AR (1:1000; N20; Santa Cruz Biotechnology), anti-DYKDDDK (1:1000; 018-22381; Wako Pure Chemicals), anti-HA tag HRP-DirecT (1:1000; 561-7; Medical and Biological Laboratories), anti-ubiquitin (1:1000; catalog #3936; Cell Signaling Technology), and anti-GAPDH (1:10,000; Millipore).

Pulse-chase labeling assay. Cells were transfected as described above; they were starved for 1 h in methionine- and cysteine-free DMEM containing 10 ng/ml NGF, 1 μg/ml doxycycline, and 1 nM DHT and were then labeled for 1 h with 150 Ci of Redivue Pro-Mix L- [^{35}S] *in vitro* cell-labeling mix (GE Healthcare) per milliliter of the culture medium. After being washed in PBS, the cells were chased for the indicated time intervals in complete medium. Immunoprecipitation was performed using equivalent amounts of protein lysates, 50 μl of protein G Dynabeads (Invitrogen), and 5 μl of anti-AR antibody (H280; Santa Cruz Biotechnology) for 10 min at room temperature. Each sample was separated by 5–20% SDS-PAGE and was analyzed by phosphorimaging (Typhoon LFA 9000 PhosphorImager; GE Healthcare) using Image Gauge software version 4.22 (GE Healthcare).

Quantitative real-time RT-PCR. Total RNA was isolated from the PC12 cells and Neuro2A cells using the RNeasy Mini kit (Qiagen) and from mouse tissues using the PureLink RNA Mini kit (Invitrogen), according to the instructions of the manufacturer. The total RNA from the cells (3 μg) and mouse tissues (2.5 μg) was reverse transcribed using SuperScript III reverse transcriptase (Invitrogen). Real-time RT-PCR was performed in a total volume of 25 μl containing 12.5 μl of 2× QuantiFast SYBR Green PCR Master Mix (Qiagen) and each primer at a concentration of 1 μM. The PCR products were detected using the iCycler system (Bio-Rad). The reaction conditions were 95°C for 5 min and then 40 cycles of 10 s at 95°C and 30 s at 60°C. As an internal standard control,

the expression of GAPDH was simultaneously quantified using the following primers: 5′-CCTGGAGAAACCTGCCAAGTAT-3′ and 5′-TGAAGTCGCAGGAGACAACCT-3′. The primers used to detect the AR were designed as described previously (Waza et al., 2005). The primers used for p62 detection were 5′-ATGCTGTCCATGGGTTTCTC-3′ and 5′-GGTGGAGGGTGCTTTGAATA-3′ for PC12 cells and 5′-CCAGTGATGAGGAGCTGACA-3′ and 5′-CATCACAGATCACATTGGGG-3′ for Neuro2A cells. The R.S.I. was computed as the signal intensity of each sample divided by the signal intensity of the control siRNA-transfected cells (see Fig. 3) and AR–24Q/$p62^{(+/+)}$ or AR–97Q/$p62^{(+/+)}$ mice (see Fig. 9).

Statistical analyses. The data were analyzed using unpaired *t* tests and *post hoc* tests (Tukey–Kramer tests) for multiple comparisons, along with the Kaplan–Meier and log-rank tests to assess the survival rate, as calculated using Statview software version 5 (Hulinks).

Results

AR is degraded via the p62-dependent autophagic pathway in cultured cells

p62 is degraded in the autophagic–lysosomal pathway through its interaction with LC3 (Komatsu et al., 2007; Ichimura et al., 2008). In addition, the AR can also be degraded by autophagy (Montie et al., 2009). To determine whether normal and mutant ARs are degraded by autophagy in cells in which the protein forms inclusions in the nucleus, as in motor neurons in SBMA, we treated an inducible PC12 cell model of SBMA that expresses full-length human AR with wild-type (AR–10Q) or mutant (AR–112Q) AR with bafilomycin A1, which is a potent inhibitor of autophagy. In this model, AR–112Q forms NIs in response to DHT, and treatment with DHT for 7 d increased the frequency of inclusions nearly threefold compared with treatment for 3 d (Walcott and Merry, 2002). Immunoblot analysis revealed a significant accumulation of monomeric wild-type (AR–10Q) and mutant (AR–112Q) AR in the PC12 cells that were treated with bafilomycin A1 after DHT treatment for 3 and 7 d; p62 also accumulated in the bafilomycin A1-treated cells (Fig. 1*A*). Bafilomycin A1 treatment also significantly increased the amount of the high-molecular-weight complex of mutant AR in the AR–112Q cells after DHT treatment for 7 d (Fig. 1*A*). Similar accumulations of AR–24Q, AR–97Q, and p62 were observed when we transiently transfected wild-type (AR–24Q) or mutant (AR–97Q) AR into Neuro2A cells and treated the cells with bafilomycin A1 (Fig. 1*B*). Accumulation of wild-type and mutant AR was similarly observed in treatment with lactacystin, which is a potent inhibitor of the ubiquitin–proteasome pathway (Fig. 1*A*, *B*). These findings suggest that the AR is degraded not only via the UPS but also via the autophagic–lysosomal pathway, and this effect occurs independently of inclusion formation in the nuclei. To examine whether AR was localized in LC3-positive cytoplasmic puncta, we cultured the PC12 cells with doxycycline, NGF, and DHT for 7 d. Immunofluorescence staining revealed that bafilomycin A1 treatment increased p62- and LC3-positive cytoplasmic puncta, which colocalized with both wild-type and mutant ARs (Fig. 1*C*). This result suggests that both wild-type and mutant ARs are degraded in the p62-dependent autophagic pathway. These findings are consistent with a previous study that reported that p62 interacted with mutant huntingtin and was degraded by autophagy (Bjørkøy et al., 2005). Nevertheless, p62 colocalized with AR–112Q in the NIs (Fig. 1*C*).

p62 interacts with the AR

p62 interacts with LC3 via a short domain of its C-terminal portion and is selectively degraded by autophagy (Ichimura et al., 2008; Ichimura and Komatsu, 2010). However, it is unclear whether p62 can interact with the AR protein. Because wild-type p62 was difficult to use in immunoprecipitation assay experiments given its propensity for aggregation, we used p62 with a PB1 (Phox and Bem1p) domain mutation (Fig. 2*B–F*). The self-oligomerization of p62 has been shown to be severely attenuated by this mutation (Lamark et al., 2003; Ichimura et al., 2008). In immunoprecipitation experiments, AR–24Q and AR–97Q coimmunoprecipitated with both endogenous and transfected p62, which suggests that p62 could either directly or indirectly recognize the AR (Fig. 2*A–G*). To determine the region of p62 that is required for the interaction with AR, we performed immunoprecipitation assay experiments using a series of p62 deletion mutants. The functional domains and exons of the corresponding mouse p62 gene were preserved in each construct (Fig. 2*E*). Deletion mutants of p62 (M6 and M7) failed to interact with the AR, whereas other mutants (M0–M5) interacted with the AR, which suggests that amino acid sequences from exon 4 (amino acids 180–225) of p62 are essential for its interaction with the AR (Fig. 2*F*). This AR–p62 interaction did not change when ubiquitin binding was disrupted using the M406V mutation in the p62 expression vector (Fig. 2*G*) (Falchetti et al., 2004). These results indicate that p62 can either directly or indirectly recognize the AR without ubiquitination and that the AR is degraded via autophagy.

Depletion of p62 promotes the accumulation of AR in a cell culture model

To determine whether depletion of p62 influences the turnover of AR, we treated the inducible PC12 cells that expressed AR–10Q and AR–112Q with either control siRNA or p62 siRNA. Immunoblot analysis revealed the accumulation of both monomeric wild-type (AR–10Q) and mutant (AR–112Q) AR after DHT treatment for 3 and 7 d and the accumulation of a high-molecular-weight complex of the mutant AR in the AR–112Q cells after DHT treatment for 7 d in the PC12 cells that were depleted of p62 ($p < 0.01$), which suggests that both wild-type and mutant ARs were degraded via p62-dependent autophagic degradation (Fig. 3*A*). Similar accumulations of AR–24Q, AR–97Q, and p62 were observed when we transiently transfected wild-type (AR–24Q) or mutant (AR–97Q) AR into Neuro2A cells and treated the cells with p62 siRNA (Fig. 3*B*). The turnover of wild-type (AR–10Q) and mutant (AR112Q) ARs was then assessed using a pulse-chase labeling assay in PC12 cells to determine whether the enhanced degradation of AR was attributable to protein degradation or to a change in RNA expression. Wild-type and mutant ARs were degraded almost equally in the absence of p62 siRNA, as reported previously (Bailey et al., 2002; Lieberman et al., 2002). In the absence of p62, wild-type and mutant ARs exhibited markedly diminished degradation (Fig. 3*C*,*D*), whereas the mRNA levels for both AR–10Q and AR–112Q were quite similar when treated with control or p62 siRNA constructs (Fig. 3*E*). Similarly, the mRNA levels for both AR–24Q and AR–97Q in Neuro2A cells were approximately equal when treated with mock or p62 siRNA constructs (Fig. 3*F*). These data indicate that deprivation of p62 influenced the autophagic degradation of both wild-type and mutant proteins without altering the mRNA levels, even in cells with NIs.

Depletion of p62 impairs the phenotypes of male AR–97Q mice

The aforementioned results suggest that endogenous p62 plays an important role in the degradation of misfolded polyQ protein in cells. We hypothesized that, if p62 contributes to the cellular

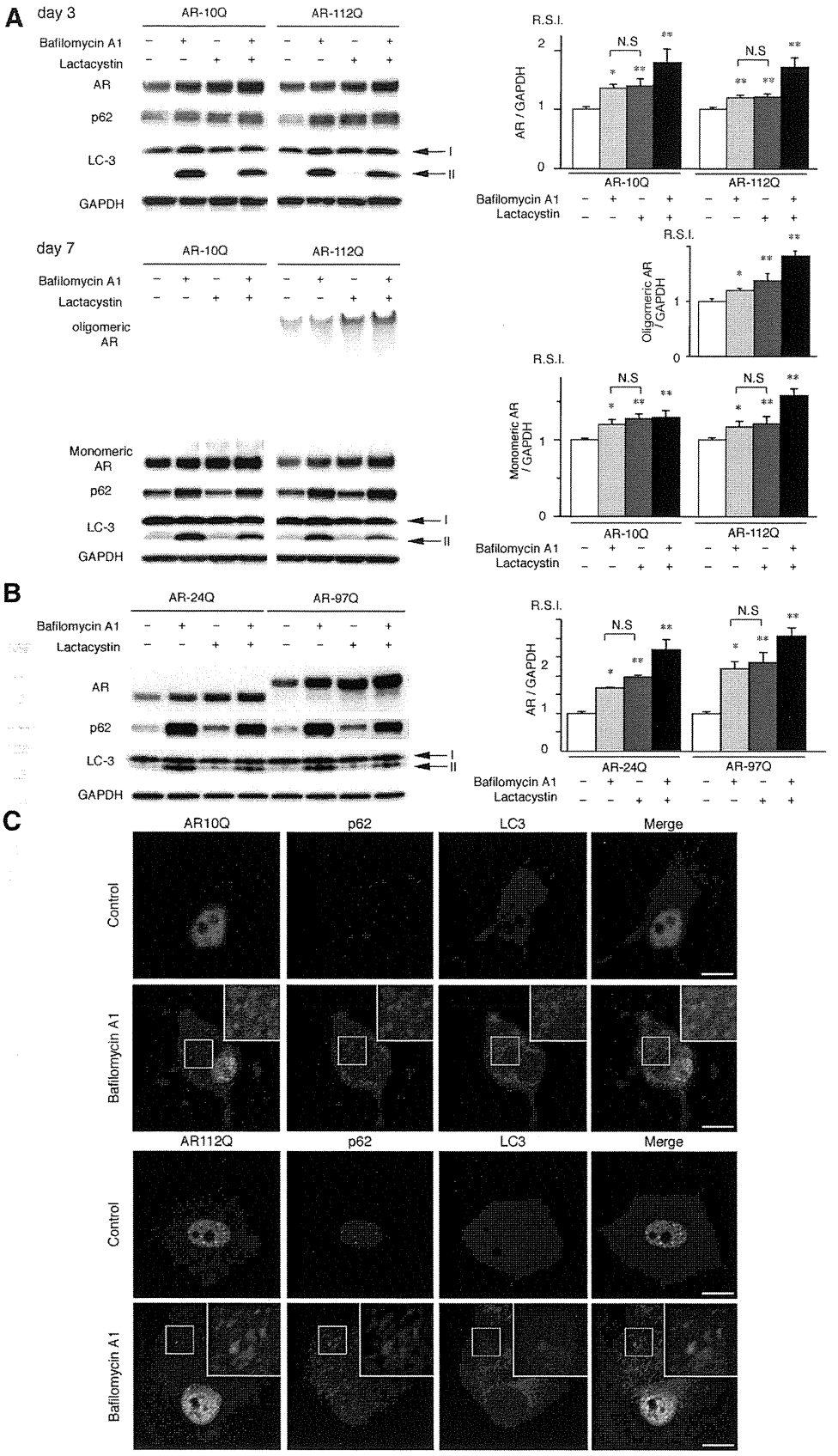

Figure 1. AR is degraded in a p62-dependent autophagic pathway. ***A***, PC12 cells that express wild-type (10Q) and mutant (112Q) AR were treated with bafilomycin A1 (20 nM) and/or lactacystin (2.5 μM) for 16 h after DHT treatment for 3 or 7 d. Immunoblot analysis was performed. ***B***, Neuro2A cells that were transfected with wild-type (24Q) and mutant (97Q) ARs were treated with bafilomycin A1 (20 nM) and lactacystin (2.5 μM) for 16 h. ***C***, Immunofluorescence for AR10Q and 112Q (green), p62 (blue), LC3 (red), and an overlay (white) of the three signals in PC12 cells for no treatment (control) and a treatment of bafilomycin A1 (20 nM). Scale bars, 10 μm. These experiments were repeated in five sets of cells, and equivalent results were obtained. All of the values are expressed as the means ± SEM ($n = 5$). *$p < 0.05$; **$p < 0.01$.

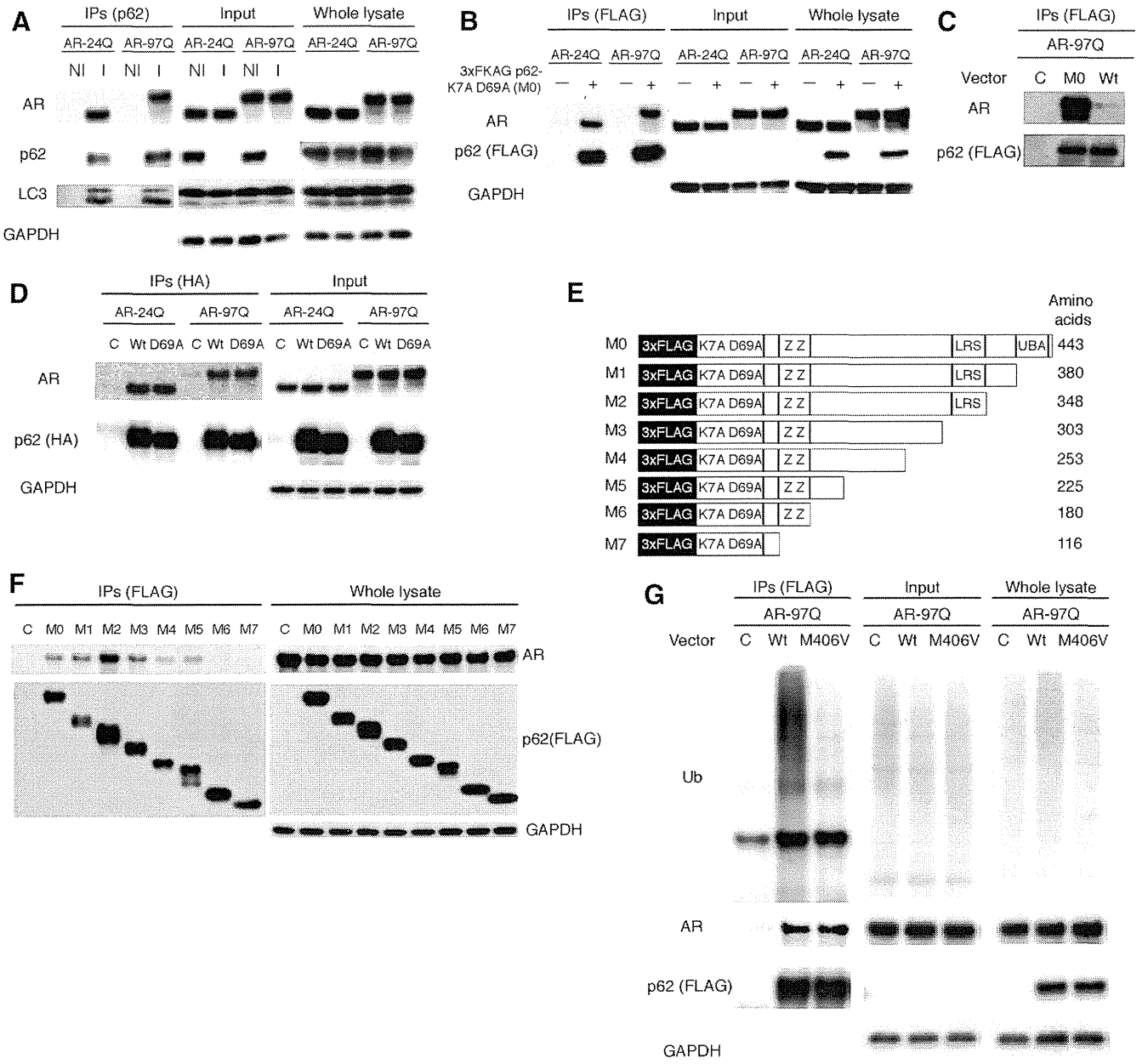

Figure 2. p62 interacts with AR. ***A***, Neuro2A cells transfected with wild-type (24Q) and mutant (97Q) AR were treated with bafilomycin A1 (20 nM) for 16 h. Immunoprecipitation was then performed with non-immune rabbit IgG (NI) or an antibody for endogenous p62 (I). ***B***, PB1 mutant p62 (M0) or wild-type p62 (Wt) and AR were cotransfected in Neuro2A cells, followed by immunoprecipitation with FLAG M2 agarose beads. Mutant p62 coprecipitated with AR, whereas the control did not show an interaction. ***C***, PB1 mutant p62 (M0) and AR were cotransfected in Neuro2A cells. Immunoprecipitation was then performed using FLAG M2 agarose beads. ***D***, p62 with an HA tag and ARs were cotransfected in Neuro2A cells. Immunoprecipitation was then performed using an HA antibody. ***E***, A schematic representation of p62 deletion mutants fused with an N-terminal 3xFLAG generated by mutagenesis. ***F***, AR–97Q and p62 mutants (M0–M7) were cotransfected, and immunoprecipitation was performed. ***G***, Mutant p62 (M406V) or wild-type p62 (Wt) and AR–97Q were cotransfected in Neuro2A cells, followed by immunoprecipitation using FLAG M2 agarose beads. IPs, Immunoprecipitations; C, control; K7A D69A, Phox and Bem1p (PB1) domain with mutations for each amino acid; ZZ, ZZ-type zinc finger; LRS, LC3 recognition sequence; Ub, ubiquitin.

quality control of the mutant polyQ protein, then reducing the expression of p62 should exacerbate polyQ disease. To test this hypothesis *in vivo*, we crossed an SBMA transgenic mouse that overexpressed the full-length human AR with either 24Q or 97Q mice (AR–24Q or AR–97Q mice) with p62 knock-outs (−/−) (Komatsu et al., 2007). Because SBMA mice (AR–97Q mice) have a small body size, a shorter lifespan, progressive muscle atrophy and weakness, reduced cage activity, and a male preponderance similar to that of human SBMA patients (Katsuno et al., 2002), we used male transgenic mice in this study. The disease progression in the AR–97Q mice that had a homozygous depletion of p62 (AR–97Q/$p62^{-/-}$) was significantly exacerbated compared with the disease progression in SBMA transgenic mice with normal p62 activity (AR–97Q/$p62^{+/+}$) and in AR–97Q/$p62^{+/-}$ mice with a heterozygous depletion of p62. Immunohistochemical studies of the spinal anterior horn and muscle using the p62-specific antibody in AR–97Q/$p62^{+/+}$ and AR–97Q/$p62^{-/-}$ mice confirmed the absence of p62 staining in the nuclei and cytoplasms of knock-out animals (Fig. 4*A–D*). Western blotting analysis confirmed the decline of p62 expression in the spinal cord and muscle of $p62^{+/-}$ mice and $p62^{-/-}$ mice (Fig. 4*E*). Mice of all three genotypes appeared to be normal until 6–9 weeks of age.

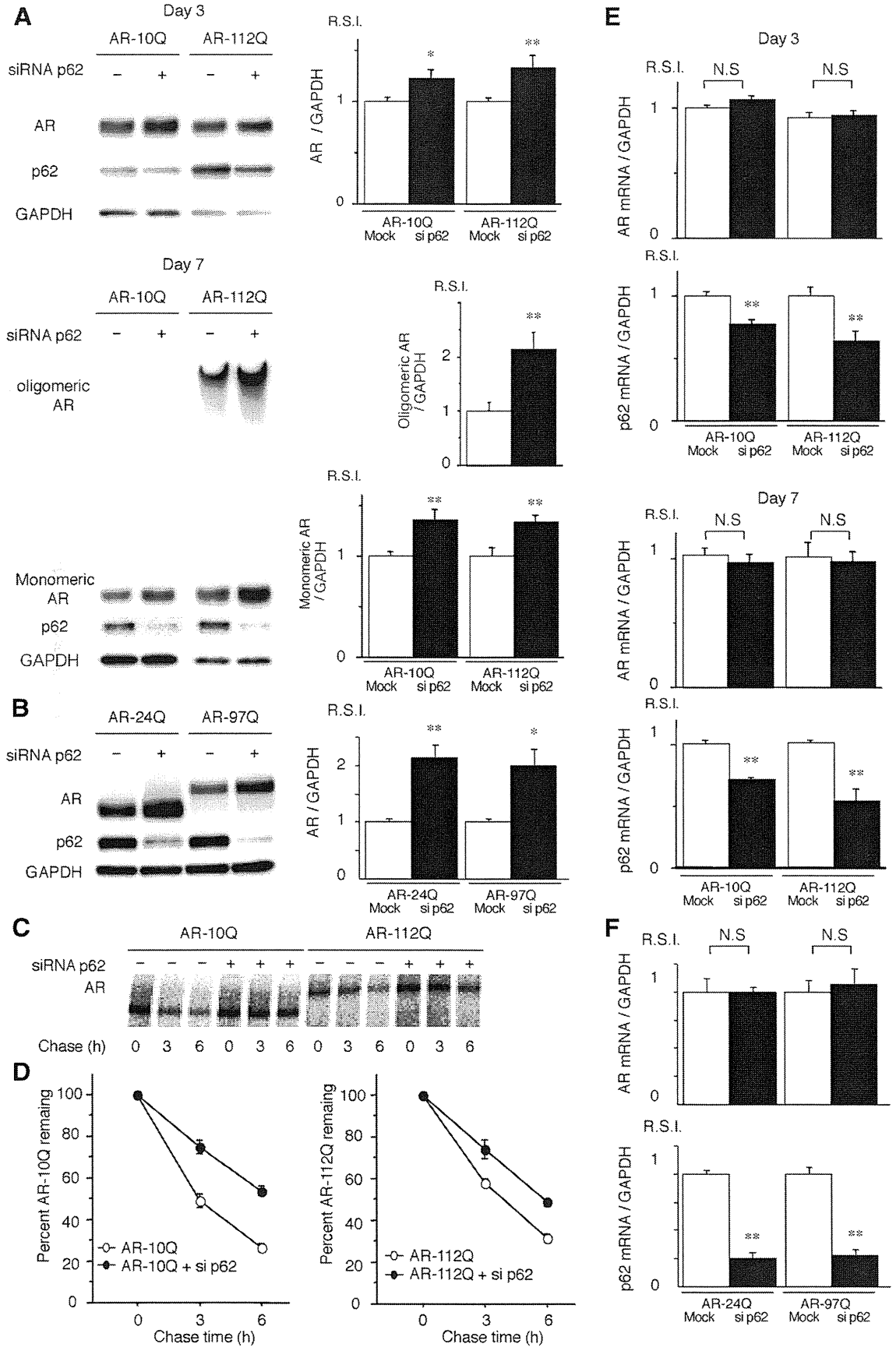

Figure 3. Depletion of p62 promotes the accumulation of AR. ***A***, PC12 cells expressing wild-type (10Q) and mutant (112Q) AR were transfected with either control or p62 siRNA. The cells were treated with DHT for 3 or 7 d. ***B***, Neuro2A cells transfected with wild-type (24Q) and mutant (97Q) AR were cotransfected with control or p62 siRNA. ***C***, Pulse-chase analysis of two forms of AR in PC12 cells. Data from one representative experiment for wild-type and mutant AR. ***D***, Pulse-chase assessment of half-life of the wild-type (left) and mutant AR (right). The percentages (*Figure legend continues.*)

However, by 10–15 weeks, the AR–97Q/$p62^{-/-}$ mice displayed prominent kyphosis, muscle weakness and atrophy, and a foot-dragging walk with foot inversion (Fig. 4*F–K*). After onset, the phenotype of the AR–97Q/$p62^{-/-}$ mice progressed rapidly to death over a 10–20 week period. By 20 weeks, only 10% of the AR–97Q/$p62^{-/-}$ mice remained alive, in contrast to ~40% of the AR97Q/$p62^{+/+}$ mice (Fig. 4*J*). Furthermore, up to 25 weeks of age, none of the AR–24Q/$p62^{-/-}$ mice showed any neurological phenotypes (data not shown).

To further characterize the motor phenotype of these mice, we performed rotarod testing for 15-week-old AR–97Q/$p62^{+/+}$ and AR–97Q/$p62^{-/-}$ mice. AR–97Q/$p62^{-/-}$ mice exhibited significant motor impairment as assessed by the rotarod task when compared with AR–97Q/$p62^{+/+}$ mice ($p < 0.05$; Fig. 4*F*). Locomotor cage activity for AR–97Q/$p62^{-/-}$ and AR97Q/$p62^{+/-}$ mice was also significantly decreased when compared with that of the AR–97Q/$p62^{+/+}$ mice ($p < 0.01$ and 0.05, respectively; Fig. 4*G*). AR–97Q/$p62^{-/-}$ mice consistently performed more poorly than the other genotypes in tasks for testing grip strength ($p < 0.01$; Fig. 4*H*). In addition, none of the genotypes were distinguishable in terms of body weight at birth. However, AR–97Q/$p62^{-/-}$ mice lost weight significantly earlier and more profoundly when compared with AR–97Q/$p62^{+/+}$ mice ($p < 0.01$; Fig. 4*I*). Depletion of p62 also significantly decreased the survival rate of SBMA mice when compared with AR–97Q/$p62^{+/+}$ mice (AR–97Q/$p62^{+/+}$ vs AR–97Q/$p62^{+/-}$, $p = 0.247$ vs AR–97Q/$p62^{-/-}$, $p = 0.007$; Fig. 4*J*). Moreover, AR–97Q/$p62^{-/-}$ mice exhibited early onset of motor weakness, with dragging legs and shorter steps when compared with AR–97Q/$p62^{+/+}$ mice (Fig. 4*K*). Although the AR–97Q/$p62^{+/-}$ and AR–97Q/$p62^{-/-}$ mice both showed phenotypic expression, the AR–97Q/$p62^{+/-}$ mice had better performance than the AR–97Q/$p62^{-/-}$ mice for most of these parameters, which suggests that the affected motor phenotype depended on the expression level of p62 rather than the genetic background.

Depletion of p62 induces the accumulation of ARs in an SBMA mouse model

We immunohistochemically examined mouse tissue samples for mutant ARs using the 1C2 antibody, which specifically recognizes expanded polyQs, and we noted a marked increase in DNS in the spinal cord (Fig. 5*A–C*) and muscles (Fig. 5*D–F*) in AR–97Q/$p62^{-/-}$ mice at 13 weeks when compared with the AR–97Q/$p62^{+/-}$ and AR–97Q/$p62^{+/+}$ mice. Quantitative assessments showed significantly more 1C2-positive cells in the spinal cord (Fig. 5*G*) and muscles (Fig. 5*H*) of AR–97Q/$p62^{-/-}$ mice when compared with AR–97Q/ $p62^{+/+}$ mice. Because wild-type and mutant ARs similarly accumulate in the absence of p62 *in vitro*, we also examined the expression of ARs in SBMA mice. Western blotting analysis of lysates from the spinal cord and muscle of AR–97Q mice revealed a high-molecular-weight mutant AR protein complex that was retained in the stacking gel as smear-shaped bands in addition to a band that could represent the monomeric mutant AR. Moreover, only the band for the wild-type monomeric AR was visible in the tissue from the AR–24Q mice (Fig. 5*I,J*). Depletion of p62 significantly increased the amount of the high-molecular-weight complex, the monomeric form of the mutant AR in the spinal cord and muscle of AR–97Q mice, and the amount of wild-type monomeric AR in AR–24Q mice (Fig. 5*I,J*). These observations indicate that p62 affects p62-dependent degradation of wild-type and mutant AR proteins via autophagy. Anti-GFAP antibody staining showed an apparent increase in reactive astrogliosis in AR–97Q/$p62^{-/-}$ mice when compared with AR–97Q/$p62^{+/+}$ mice in the spinal anterior horn (Fig. 5*K,L*). Western blotting analyses using an antibody against GFAP revealed that depletion of p62 upregulated GFAP, which indicates that the depletion of p62 exacerbated the neurodegenerative changes (Fig. 5*M*). Muscle histology and weight measurement also revealed significant exacerbation of muscle atrophy in AR–97Q/$p62^{-/-}$ mice compared with AR–97Q/$p62^{+/+}$ mice (Fig. 5*N–P*). Depletion of p62 did not influence the expression of total ubiquitinated proteins in the spinal cord and muscle of AR–24Q and AR–97Q mice, as determined by ubiquitin staining of Western blots (Fig. 5*Q*) and histology (data not shown).

p62 overexpression ameliorates phenotypes in male AR–97Q mice

To test whether increased expression of p62 provides protective effects in AR–97Q mice, we generated transgenic mice that overexpressed full-length human p62 with a C-terminal HA tag under the control of a cytomegalovirus enhancer and a chicken β-actin promoter (Fig. 6*A*). The promoter used for this transgenic mouse was the same as that used in the SBMA model mice. Among 10 available mouse lines, we established four that expressed p62 in the spinal cord and skeletal muscle, and we examined the effects of the overexpressed p62 on mouse phenotypes. Western blotting analysis revealed that p62 expression in the spinal cords of $p62^{(tg/+)}$ mice was fourfold higher than the expression of endogenous p62 in wild-type mice. In muscle, p62 expression was 12-fold higher in $p62^{(tg/+)}$ mice compared with wild-type mice (Fig. 6*B*). Immunohistochemical studies performed on $p62^{(tg/+)}$ mouse tissue using an anti-HA tag antibody confirmed that spinal anterior horn neurons and muscle cells expressed p62. Moreover, p62 protein was distributed in the cytoplasms and nuclei of the spinal anterior horn neurons, glial cells, and muscles (Fig. 6*C,D*). Up to 35 weeks of age, none of the hemizygous transgenic mice that overexpressed p62 presented any neurological phenotypes, as assessed by the rotarod task, cage activity, grip strength, and body weight (data not shown). Histological examination at 35 weeks did not reveal any detectable effects on neuronal cell morphology, neuronal cell number, or muscle structure (data not shown). These studies indicate that overexpression of human p62 alone does not impair neuronal development or motor function.

We crossed the AR–24Q and AR–97Q mice with mice that overexpress human p62 (p62 1–1 line) to generate hemizygotic AR–24Q/$p62^{(tg/+)}$ and AR–97Q/$p62^{(tg/+)}$ mice and AR–24Q/$p62^{(+/+)}$ and AR–97Q/$p62^{(+/+)}$ mice for use as controls. The AR–97Q mice that overexpressed p62 (AR–97Q/$p62^{(tg/+)}$) demonstrated amelioration of the disease course after 18 weeks of age (Fig. 6*E–I*). In addition, AR–97Q/$p62^{(tg/+)}$ mice showed improvements in their motor impairment, as assessed by the rotarod task at 25 weeks ($p < 0.05$; Fig. 6*E*). Locomotor cage activity of the AR–97Q/$p62^{(tg/+)}$ mice was also significantly increased at 25 weeks when compared with that of the AR–97Q/$p62^{(+/+)}$ mice ($p < 0.05$; Fig. 6*F*). Furthermore, grip strength was stronger in the AR–97Q/$p62^{(tg/+)}$ mice than in the control mice ($p < 0.05$; Fig. 6*G*), and AR–97Q/$p62^{(+/+)}$ mice lost weight significantly earlier and more profoundly than the AR–97Q/

←

(*Figure legend continued.*) of wild-type (10Q) and mutant (112Q) remaining in the presence (●) and absence (○) of p62 siRNA are indicated. ***E***, Real-time RT-PCR for wild-type (10Q) and mutant (112Q) AR mRNA normalized to GAPDH levels in PC12 cells. ***F***, Real-time RT-PCR for wild-type (24Q) and mutant (97Q) AR mRNA normalized to GAPDH levels in Neuro2A cells. These experiments were repeated in five sets of cells, and equivalent results were obtained. All of the values are expressed as the means ± SEM ($n = 5$). *$p < 0.05$; **$p < 0.01$.

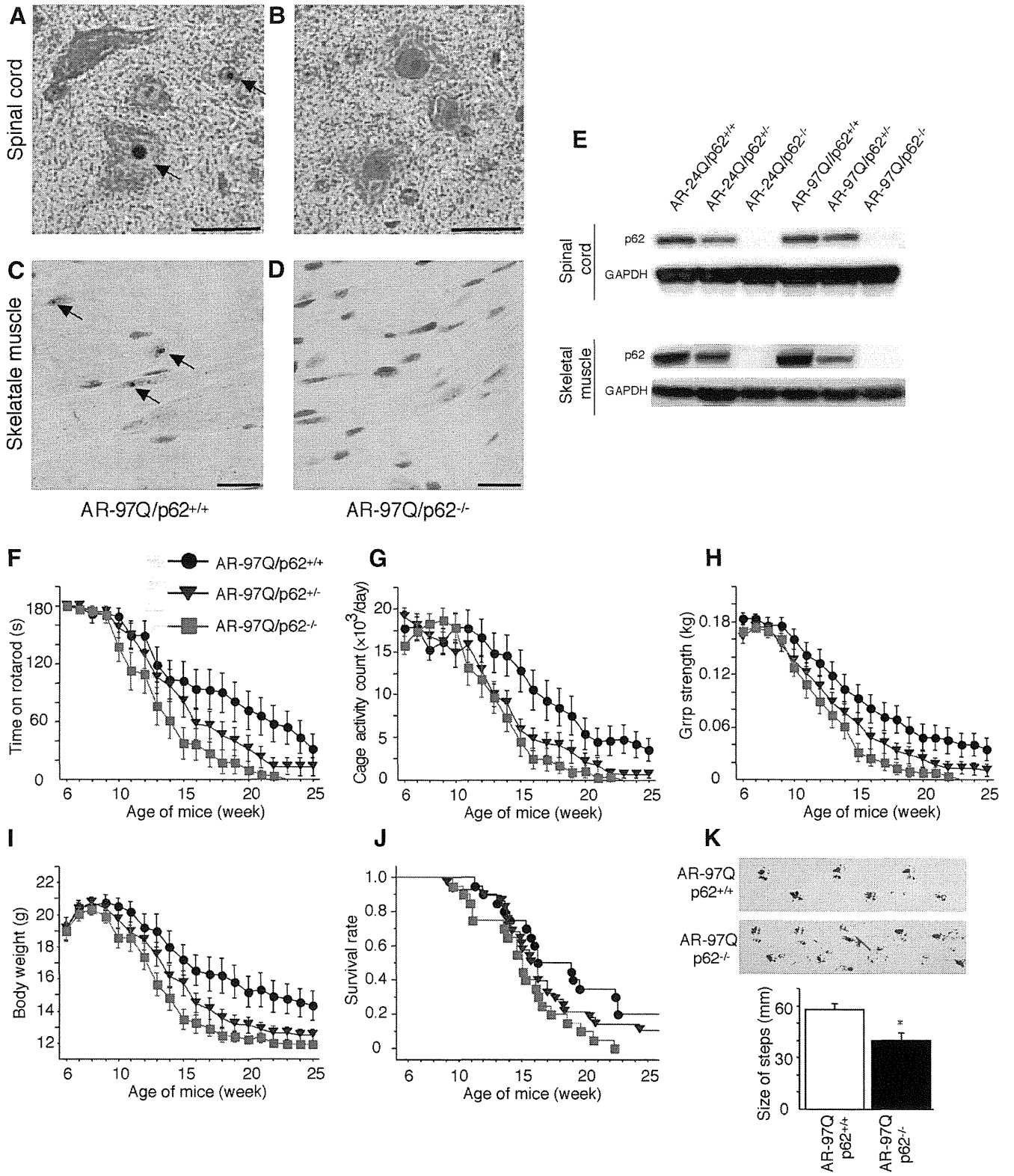

Figure 4. Depletion of p62 impairs behavioral and visible phenotypes in male AR–97Q mice. ***A–D***, p62 immunohistochemistry in the spinal anterior horn (***A***, ***B***) and skeletal muscle (***C***, ***D***) of 25-week-old AR–97Q/$p62^{+/+}$ (***A***, ***C***) and 13-week-old AR–97Q/$p62^{-/-}$ (***B***, ***D***) mice counterstained with Mayer's hematoxylin. p62 immunoreactivity was localized to the nuclei and cytoplasm, with NIs (arrow) in the anterior horn cells and skeletal muscle. Scale bars, 20 μm. ***E***, Western blotting analysis of p62 expression in the total spinal cord and muscle protein lysates from the indicated mice immunolabeled with antibodies against p62. ***F–J***, Rotarod task (***F***), cage activity (***G***), grip strength (***H***), body weight (***I***), and survival rate (***J***) of the AR–97Q/$p62^{+/+}$(●; $n = 20$), AR–97Q/$p62^{+/-}$(▼; $n = 28$), and AR–97Q/$p62^{-/-}$ (■; $n = 20$) mice. Although none of the parameters tested at 15 weeks revealed significant differences between AR–97Q/$p62^{+/-}$ and AR–97Q/$p62^{+/+}$ mice, the AR–97Q/$p62^{+/-}$ mice performed more poorly than the AR–97Q/$p62^{+/+}$ mice in all of the parameters. ***K***, Footprints of representative 13-week-old AR–97Q/$p62^{+/+}$ and AR–97Q/$p62^{-/-}$ mice. The front paws are indicated in blue, and the hindpaws are indicated in red. Values are expressed as the means ± SEM. *$p < 0.05$.

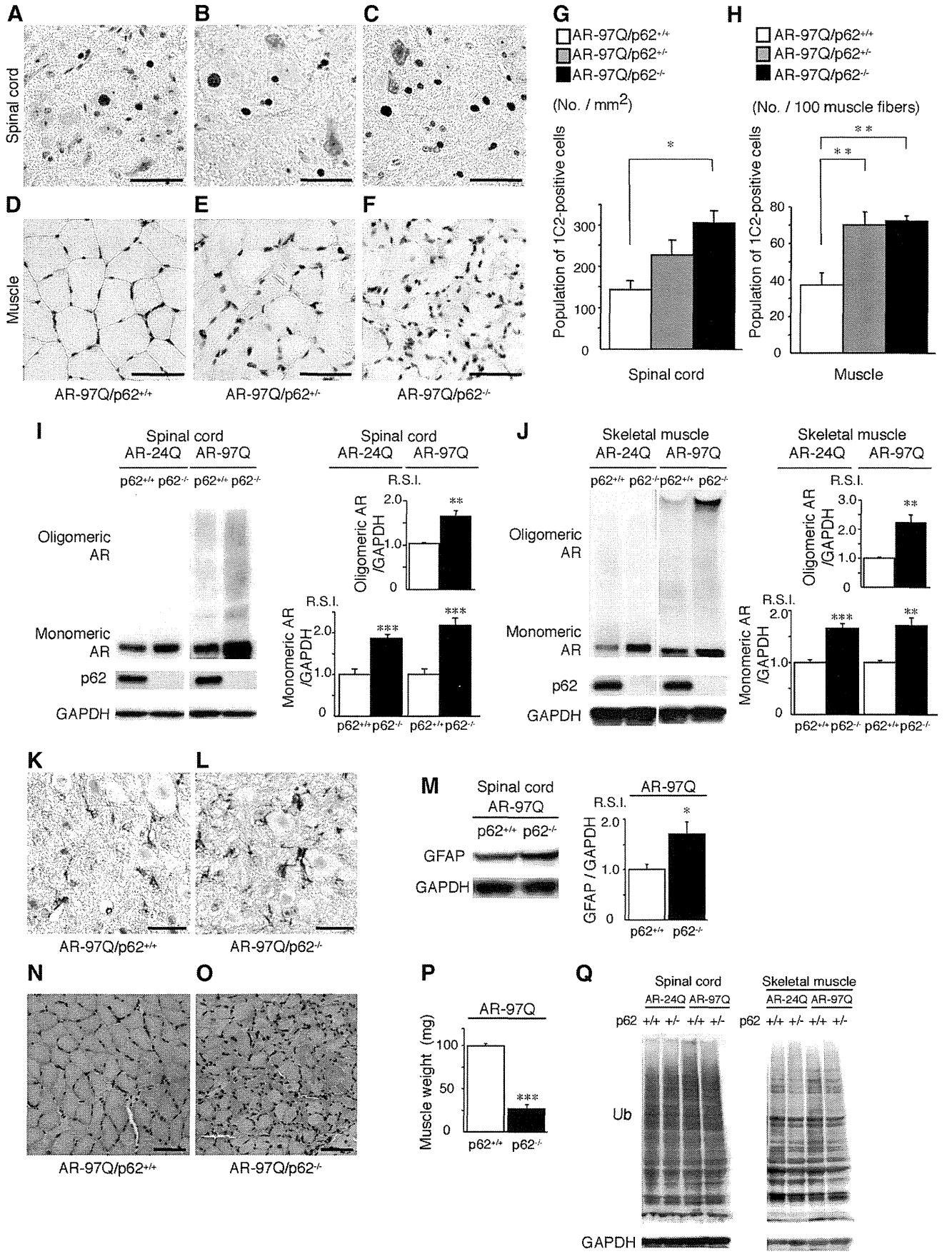

Figure 5. Depletion of p62 induces the accumulation of AR in an SBMA mouse model. ***A–F***, PolyQ immunohistochemistry (1C2) in the spinal anterior horn (***A–C***) and muscle (***D–F***) of 13-week-old AR–97Q/*p62*$^{+/+}$, AR–97Q/*p62*$^{+/-}$, and AR–97Q/*p62*$^{-/-}$ mice. Scale bars, 50 μm. ***G***, ***H***, Quantitative assessment of 1C2 staining in the spinal ventral horn (***G***) and muscle (***H***). (*Figure legend continues.*)